U. Walzer and R. Hendel. A new convection-fractionation model for the evolution of the principal geochemical reservoirs of the Earth's mantle. Phys. Earth Planet. Int., 112:211-256, 1999.

A new convection–fractionation model for the evolution of the principal geochemical reservoirs of the Earth's mantle

Uwe Walzer , Roland Hendel

Institut für Geowissenschaften, Friedrich-Schiller-Universität, Burgweg 11, 07749 Jena, Germany

Received 24 March 1998; received in revised form 6 January 1999; accepted 6 January 1999

Abstract

There are geochemical reservoirs (CC, DM, PM, EM1, EM2, HIMU) in the Earth's mantle and crust. They are distinguished by their isotopic and chemical abundance ratios and they arise from the combination of partial melting, segregation, ascent of the melt, differentiation of the melt, and lateral transport. The fractionation generates the chemical and isotopic diversity, while the solid-state convection works toward homogenization in particular in mantle areas with high gradient of creeping velocity perpendicular to the velocity vector. The thermal and chemical evolution of the Earth's mantle and crust has been modeled simultaneously by a fractionation mechanism plus 2D-FD Oberbeck–Boussinesq thermal convection. In contrast with the published model K1 [Walzer, U., Hendel, R., 1997a. Time-dependent thermal convection, mantle differentiation and continental-crust growth. Geophys. J. Int. 130, 303–325; geological interpretation: Walzer, U., Hendel, R., 1997b. Tectonic episodicity and convective feedback mechanisms. Phys. Earth Planet. Interiors 100, 167–188], layered convection is *not* an assumption but the mineral phase changes are introduced for 410 and 660 km depth using customary values of the Clapeyron slope, the density contrast, etc. So we have heat sources and sinks at 410 and 660 km, respectively, in addition to the usual Rayleigh number, Rq, for internal heating by radioactivity and bottom heating at the core–mantle boundary (CMB). The viscosity is a function of the temperature field and the pressure. Segregation takes place if the asthenospheric viscosity falls below a certain threshold. Oceanic plateaus, enriched in incompatible elements, develop leaving behind depleted parts of the mantle (DM). The resulting inhomogeneous heat-source distribution generates a first feedback mechanism. A growing continent is produced by accretion and further fractionation, consuming the older oceanic plateaus. The lateral movability of the growing continent causes a second feedback mechanism. The mentioned mechanisms generate acceptable distributions of the convective vigor and of the growth of juvenile continent material over the time axis. These distributions are stable for a moderate variation of the parameters only. The solutions of the system of differential equations show acceptable values for the distributions of the temperature, viscosity, heat flow, mantle-creep velocity and the continent's velocity. The following new result is insensitive to a strong variation of Rq: After an initially rather complex mixing process of the depleted parts and the pristine parts of the mantle, we arrive at a mainly depleted upper half of the mantle including the uppermost parts of the lower mantle and a predominantly pristine lower half of the mantle in the Phanerozoic at the latest. There is no sharp interface between the halves.

1. Introduction

1.1. Aim

It is amazing that the interaction between the following two fields of work is weak until now. On the one hand we have the modeling of thermal mantle convection and mantle-evolution modeling, on the other hand there is a growing number of geochemical papers on reservoirs in the mantle and the crust. The chemical composition of MORB is surprisingly uniform. This statement applies both for the gross composition and for the incompatible elements. The relative independence of MORB composition on the location of the sample can be explained by the uniformity of the MORB source (DM). This source is situated immediately beneath the lithosphere, at least under the oceanic lithosphere. Therefore we observe only a slight contamination. Caused by its low viscosity, the asthenospheric convection generates a thoroughly mixed reservoir. The MORB source (called residuum 1 according to Hofmann, 1988) is depleted in incompatible elements. The missing amount of the incompatible elements is now resident in the continental crust (CC). So, DM and CC are complementary reservoirs. The pristine mantle (PM) is abundant in large-ion lithophile elements and by the way also in volatiles. Its volume has the same order of magnitude as residuum 1. The geochemists presume that PM is situated deeper than DM. This supposition can be confirmed for the Phanerozoic by our computations to come to the point. The existence of the mentioned reservoirs would be puzzling in the case of unrestrained whole-mantle convection. Mantle convection has the effect of diminution, blurring and, after all, annihilation of the differences of the chemical composition of the reservoirs by stirring whereas the following processes act as antagonists: formation of partly molten systems, enrichment of the melt with U, Th and K, other segregation, transport and differentiation of the melt, low tendency of rocks with low zero-pressure density to perpetual subduction. There are today the three principal geochemical reservoirs (CC, DM, PM) and some minor reservoirs (EM1, EM2, HIMU), yet, in spite of the 4.57×10^9 years of the Earth's evolution and of convective stirring. This fact *and* all essential features of mantle convection should be deducible from *one* geophysical model system with acceptable initial and marginal conditions. Of course we have to abstract from a lot of known facts, e.g., from the heterogeneity of the CC. In contrast to Walzer and Hendel (1997a,b), we want to model the origin, the evolution and the present existence of the three principal geochemical reservoirs without introducing physical compulsory conditions.

1.2. Mantle convection and thermal evolution

The attempts to explain the movements of the lithospheric plates and the orogenesis by thermal convection can be traced back to Schwinner (1920). He thought that these processes are caused by thermal buoyancy in the mantle and he designated the radioactive decay as the principal energy source of it. At that time of course a modern numerical modeling was not feasible because of the missing computers. Until the review of Schubert (1979), the view was gradually gaining ground that thermal solid-state convection is the driving mechanism behind the mentioned processes, that the mantle rheology is heavily dependent on temperature and pressure and that planetary convection with high Rayleigh numbers is fully three-dimensional and time-dependent. Because Schubert investigated the Earth from the viewpoint of thermodynamics and fluid mechanics he concluded that the mantle has forgotten is initial conditions, that is, no matter whether the Earth's start was hot or cold, the mantle would arrive at the present thermal state. It is our opinion that now the time is ripe to exclude some initial-state models in consideration of geochemical and isotopic findings and of coagulation models. A mean formation time of the Earth of about 12 Ma can be concluded from the coagulation models of Wetherill (1986). The widely held coagulation equations have, however, a serious defect: in some cases the total mass of the system is not conserved (Tanaka and Nakazawa, 1994). Therefore, Tanaka and Nakazawa (1993) proposed a new stochastic coagulation equation in order to avoid this shortcoming. Williams and Wetherill (1994) described the interplay between coagulation and catastrophic fragmentation during the accretion of the Earth. The mentioned mean formation time of the Earth is not essentially altered by these new

findings. The application of extinct nuclides (^{129}I, ^{244}Pu, ^{182}Hf and ^{146}Sm) to the early differentiation processes (Jacobsen and Harper, 1996) established some partial results for the earliest time of the Earth's evolution (4.57–4.25 Ga). A time span of accretion of the Earth and core formation between 2 and 15 Ma has been concluded from the Hf–W system. That is why we took the subdivision of the Earth into the Earth's core and a primordial silicate mantle as a given initial state of our model for the Earth's mantle evolution. The chemical fractionation of the CC out of the primordial mantle is, however, a long lasting process. Although it has a strong initial phase, that fractionation continues to operate over the whole Earth history culminating in peaks of orogenetic activity. In those time spans we observe not only the accretion of palingene rhyolithic material to the continent but also a real increase in juvenile continent material.

Using the parameterization of the convective heat transport, Christensen (1985) investigated evolution models for the Earth. He came to the conclusion that the heat flow depends much weaker on the mantle temperature than earlier expected. The generation of additional convective instabilities by mineral phase transitions is an old idea (Vening Meinesz, 1956). Models including that idea have been further developed in the last years: Christensen and Yuen (1985) found that the endothermic phase transition in 660 km depth gives rise to a mantle flush instability. The question as to whether there is whole-mantle convection or layered convection has been answered by a compromise solution: There is two-layer convection with episodic avalanches or breakthroughs of the convective currents through the 660 km discontinuity. A lot of papers deal with that topic (Machetel and Weber, 1991; Honda et al., 1993; Steinbach et al., 1993; Tackley, 1993; Solheim and Peltier, 1994).

It has often been overlooked that the influence of pressure and temperature dependencies of the viscosity on that question is even stronger. This result has been found by Bunge et al. (1997) using a three-dimensional model of convection in a spherical shell. In this model, the viscosity does not depend on the temperature though but only on the pressure. Walzer and Hendel (1997a,b) gathered experience of the same kind introducing a 2D-FD model of the Earth's evolution with a rheology depending not only on the pressure but also on the temperature field. The model includes the emergence of oceanic plateaus and a depleted mantle reservoir by chemical differentiation. The evolution of the global magmatism as a function of time has been modeled by a convection–segregation model. Spohn and Breuer (1993) had developed interesting differentiation models on CC growth before. They based on parameterized equations in contrast to the model by Walzer and Hendel (1997a,b). Schmeling and Bussod (1996) examined the generation of partial melts in the continental asthenosphere presuming a non-Newtonian rheology of olivine dependent on temperature and pressure. In the model a strongly time-dependent convection developed. Partially molten areas of the asthenosphere appeared with an episodicity of 5 to 10 Ma. The melt fractions ranged between 0 and 2% for a dry solidus and between 2 and 4% for a water-undersaturated solidus using a continental heat flow of 53.3 mW m^{-2}. The influence of sublithospheric mantle currents on plate tectonics has been studied before by Schmeling and Marquart (1993).

1.3. Geochemical reservoirs and some preparatory explanations

Our present model (cf. Section 2) starts from the presupposition that the Earth's core and the silicate mantle did not exchange material but only energy over the main part of the Earth's history. Of course in the mentioned 2 to 15 Ma initial period, no chemical isolation can be expected but this early period has not been modeled. The reason for our assumption is the observation that the abundances of siderophile elements did not essentially change in mantle rocks since 4.0×10^9 years (Delano and Stone, 1985; Newsom et al., 1986; Jochum et al., 1993; O'Neill and Palme, 1998). The observed discontinuities in the radial distribution of the seismic velocities and the density at 410 and 660 km depth permit only small deviations in the abundances of the chemical main components expressed as oxides. The error bars even allow the assumption of an equal cross composition of asthenosphere, transition layer and lower mantle. However, the mantle as well as the crust are subdivided in geochemical reservoirs according to their abundance of incompatible ele-

ments. Already early the conception emerged that the different isotopic composition of mantle-derived basalts can be explained by mixing of depleted mantle reservoirs and primordial ones (Jacobsen and Wasserburg, 1979; O'Nions et al., 1979; Allègre et al., 1980). The most relevant heat-producing elements (U, Th and K) are incompatible. Therefore, the growth of the depleted mantle and of its complementary reservoir, CC, has an influence on the mode of thermal mantle convection and on the thermal evolution of the mantle. That is why we have developed the present geodynamic model (called K2A) where we presupposed only the possibility of the division in reservoirs and the abundance values (called $a_{\mu\nu}$ in our notation) of Hofmann (1988) as a base of our computations. In this paper we neglected the smaller geochemical reservoirs (residuum 2, EM1, EM2, HIMU, etc.) in order to describe not only the mechanism geochemically and to compute it from the geodynamic point of view but also to understand the mechanism from the physical standpoint. The most important reservoir is the depleted mantle (Hofmann's residuum 1) which is accessible by peridotite samples. In a plot of the normalized concentrations of the elements vs. compatibility an opposite slope is observed for CC and DM. The conclusion is that CC and DM arose from PM by one or two stages of chemical segregation and differentiation. Total homogenization of DM plus CC would give the result of a new PM minus a certain amount of volatiles. On the other hand the oceanic crust results from fractionation of DM near the divergent plate boundaries leaving behind an even more depleted reservoir. Hofmann (1988) christened it residuum 2, O'Neill and Palme (1998) called it residual depleted mantle.

The present paper describes an interlocked model of thermal mantle convection plus chemical segregation and differentiation. The generation of CC and DM from PM is interweaved with a two-dimensional Oberbeck–Boussinesq FD convection model. The evolution of the Earth's mantle and crust is controlled by thermodynamically irreversible processes: the radioactive decay of ^{238}U, ^{235}U, ^{232}Th and ^{40}K, thermal conduction and convection, etc. The four abundances $a_{\mu\nu}$ of the mentioned radionuclides and the viscosity are neither constants nor functions of the depth only but they evolve according to a system of differential equations (conservation equations, constitutive equations, fractionation law) as functions of the location vector and the time t. The viscosity is assumed to be a function of the temperature field and the activation enthalpy. The concentrations of the radionuclides are represented by tracers which are carried by the creep of the solid rock matrix. Special alteration of the assignment of the abundance values to the tracers takes place only of the viscosity sinks below a certain critical value in a sufficiently big area of the asthenosphere. This has been done in order to model the ascent of molten rocks which carry elevated abundances of heat-producing elements.

2. Theory and development of the geophysical model

2.1. Theory

We treat the two-dimensional time-dependent mantle convection with predominantly internal heating and little heating from below. The internal heat sources are not only trailed by the solid-state creeping in the mantle but also episodically redistributed by partial melting, segregation, rise and chemical differentiation of the melt. We use a box with an aspect ratio three and an infinite Prandtl number fluid. The convection is driven by buoyancy forces which are produced mainly by density differences due to thermal expansion but also by density differences generated by lattice changes of the two mineral phase transitions in 410 and 660 km depth. To model the mantle convection realistically, the shear viscosity η has to be introduced as a function of pressure p and temperature T. More about that can be found at the end of this section. We assume free slip boundaries at top and bottom and periodic lateral boundaries (Gottschaldt, 1997). The first two assumptions are vindicated by the large viscosity contrasts between crust and ocean and between lower mantle and outer core. In spite of the 26% growth of the solar luminosity during the 4.57×10^9 years of the Earth's existence, it is legitimate to suppose a constant surface temperature since at least 3.8×10^9 years. For details about it, see Section 3.2 of Walzer and Hendel (1997b). Mainly, it was the entirety of

Table 1
Data on major heat-producing isotopes

Isotope	^{40}K	^{232}Th	^{235}Th	^{238}U
ν	1	2	3	4
τ_ν [Ma]	2015.3	20212.2	1015.4	6446.2
$H_{0\nu}$ [W kg^{-1}]	0.272×10^{-3}	0.0330×10^{-3}	47.89×10^{-3}	0.1905×10^{-3}
$a_{\mathrm{if}\nu}$	0.000119	1	0.0071	0.9928

organisms which works as a thermostat by reducing the mass of carbon dioxide in the atmosphere through the deposition of limestone and dolomite, to a minor degree also of coal and mineral oil. At the core–mantle boundary (CMB), however, there is no thermostat. The decrease of heat in the mantle is caused by convection, the production of heat is brought on by radioactive decay. Heat transport out of the mantle–crust system and radioactive decay are opponents but they do not guarantee the constancy of the temperature at the CMB. Because of the persistent existence of the geomagnetic dynamo with a constant order of magnitude of the dipole moment, we assume a constant heat flow at the CMB, $q_{\mathrm{CMB}} = 20$ mW m^{-2}. On the other hand, the bottom temperature $T_{\mathrm{CMB}} = T_{\mathrm{CMB}}(x,t)$ depends on the time t and on x, the horizontal component of the location vector. The mentioned assumption is better suited to describe the Earth's thermal evolution than the assumption T_{CMB} = const. The arguments for this assumption can be found in Appendix A.

We presume that there are today five main reservoirs in the mantle–crust system which have different abundances of the major heat-producing elements (cf. Table 2). However, we take into account only the PM (1), the CC (3), and (4) the residuum 1 or DM. Reservoirs of minor volume are neglected. Table 1 is a list of quantities of the four major heat-producing isotopes: τ_ν denotes the decay time or the $1/e$ life, $H_{0\nu}$ is the specific heat production of the νth radionuclide 4.55×10^9 years ago, $a_{\mathrm{if}\nu}$ is the isotopic abundance factor. The specific heat production for *one* reservoir is computed from

$$H = \sum_{\nu=1}^{4} a_{\mu\nu}\, a_{\mathrm{if}\nu}\, H_{0\nu} \exp(-t/\tau_\nu) \qquad [\mathrm{D}] \qquad (1)$$

The bracketed D means that the equation contains dimensional quantities. The geochemical reservoirs are represented by tracers. If there are tracers of only *one* reservoir in the surrounding rectangle around a grid point, then we take the abundances $a_{\mu\nu}$ of this reservoir from Table 2 in order to compute the value H of the grid point. If there are tracers of different reservoirs then we determine the H of the grid point by working out the weighted arithmetic means of the abundances and inserting them into Eq. (1). We want to non-dimensionalize the heat production density Q which is measured in W m^{-3}. For this we need a quantity $Q_0 = H_0 \rho_0$ using $\rho_0 = 3340$ kg m^{-3} and

$$H_0 = \sum_{\nu=1}^{4} a_{\mu\nu}\, a_{\mathrm{if}\nu}\, H_{0\nu} \exp(-t_{\mathrm{h}}/\tau_\nu) \qquad [\mathrm{D}] \qquad (2)$$

where $t_{\mathrm{h}} = (1/2)(4550$ Ma) and the $a_{\mu\nu}$ of Type 1 tracers.

Table 2
The abundances $a_{\mu\nu}$ of the major heat-producing elements according to Hofmann (1988)

Marker index	(1)	(2)	(3)	(4)	(5)
Reservoir	Primitive mantle (ppm)	Oceanic crust (ppm)	Continental crust (ppm)	Res 1 (ppm)	Res 2 (ppm)
K	258.2	883.7	9100	201.48	161.98
Th	0.0813	0.1871	3.5	0.0594	0.0529
U	0.0203	0.0711	0.91	0.0146	0.0112

Now we introduce non-dimensional variables with primes. The primes are omitted starting from Eq. (12) except for γ'. The dimensional variables are on the left-hand side of Eq. (4). The conversion parameters and their description are listed in Table 3. The origin of the coordinate system is situated in the left lower corner of the box which represents the mantle. The scaling Rayleigh number, Rq, for heating from within and from below is

$$\mathrm{Rq} = \frac{\rho_0 \alpha g h^3}{\kappa \eta_0} \frac{(Q_0 h + q_{\mathrm{CMB}})\, h}{k} \qquad [\mathrm{D}] \tag{3}$$

where k is the thermal conductivity defined by $k = \kappa c_p \rho_0$. The meaning of the magnitudes can be found in Table 3. Optionally Rq or the reference viscosity η_0 is a given quantity. We scale the heat production per volume as follows:

$$Q = Q_0 Q' \qquad [\mathrm{D}]. \tag{4}$$

For the introduction of further non-dimensional variables, see Appendix B. Primes represent the non-dimensional variables. They are omitted in equations without the remark [D].

The transition pressure p_{tk} of the kth phase transition is

$$p_{tk} = p_{0k} + \gamma_k T \qquad [\mathrm{D}] \tag{5}$$

where p_{0k} is the transition pressure for vanishing temperature T. The excess pressure π_k is determined by

$$\pi_k = p - p_{0k} - \gamma_k T \qquad [\mathrm{D}]. \tag{6}$$

The buoyancy is influenced by the density Eq. (7). Additional to the thermal expansion, density contrasts $\Delta\rho_k$ have been introduced at the kth phase transition.

$$\rho = \rho_0 (1 - \alpha T + \Gamma \Delta\rho_k / \rho_0) \qquad [\mathrm{D}] \tag{7}$$

where

$$\Gamma(\pi_k) = \frac{1}{2}\left(1 + \tanh\frac{\pi_k}{d_k}\right). \tag{8}$$

Γ is a measure of the relative fraction of the heavier phase. It is a function of pressure p and temperature T. The form of Eq. (8) has been proposed by Richter (1973). Of course, we could introduce also another

Table 3
Further model parameters

Parameter	Description	Value
h	Depth of the convecting layer	2.891×10^6 m
h_1	Depth of the exothermic phase boundary	4.10×10^5 m
h_2	Depth of the endothermic phase boundary	6.60×10^5 m
g	Mean gravitational acceleration in the mantle	9.94 m s^{-2}
ρ_0	Reference density	3340 kg m^{-3}
c_p	Specific heat at constant pressure	1000 J kg^{-1} K^{-1}
κ	Thermal diffusivity	10^{-6} m^2 s^{-1}
q_{CMB}	Heat flow at the core–mantle boundary	0.02 W m^{-2}
t_h	Half of the time span of the mantle's evolution	2275 Ma
α	Coefficient of thermal expansion	3.14×10^{-5} K^{-1}
γ_1	Clapeyron slope for the olivine–spinel transition	$+3 \times 10^6$ Pa K^{-1}
γ_2	Clapeyron slope for the spinel–perovskite transition	-4×10^6 Pa K^{-1}
f_{a1}	Non-dimensional density jump for the olivine–spinel transition	0.08
f_{a2}	Non-dimensional density jump for the spinel–perovskite transition	0.10
d_1	Non-dimensional transition width for the olivine–spinel transition	0.05
d_2	Non-dimensional transition width for the spinel–perovskite plus magnesiowüstite transition	0.05
R	Gas constant	8.31441 J mol^{-1} K^{-1}
E_0	Activation energy	4.00×10^5 J mol^{-1}
V_0	Activation volume	6.1×10^{-6} m^3 mol^{-1}
η_{01}	Viscosity constant in the mantle except transition layer and lithosphere	1×10^7 Pa s
η_{02}	Viscosity constant in the transition layer	1×10^9 Pa s
η_{lith}	Viscosity of the lithosphere	5×10^{22} Pa s
η_{thr}	Threshold viscosity	2.1×10^{20} Pa s

smooth curve as a modification of the step function. Neglecting the non-hydrostatic part of the pressure we receive

$$\frac{\mathrm{d}\Gamma_k}{\mathrm{d}\pi_k} = \frac{1}{2d_k}\left(1 - \tanh^2\frac{\pi_k}{d_k}\right). \tag{9}$$

This curve has its maximum at $\pi_k = 0$. We have to substitute

$$\pi_k = z_k - z - \gamma_k T \tag{10}$$

and

$$z_k = (h - h_k)/h \qquad \text{for } k = 1,2. \tag{11}$$

The formulae (5) to (11) have been introduced in a similar form by Christensen and Yuen (1985). The quantity z in Eq. (10) is the non-dimensional vertical component of the location vector. h_k, d_k and other quantities are defined in Table 3. Since the dependence of the viscosity η on temperature and pressure is very important for mantle convection, the *conservation of momentum* is expressed by

$$4\frac{\partial^2}{\partial x \partial z}\left[\eta(T,p)\frac{\partial^2\psi}{\partial x\partial z}\right] + \left(\frac{\partial^2}{\partial z^2} - \frac{\partial^2}{\partial x^2}\right) \times \left[\eta(T,p)\left(\frac{\partial^2\psi}{\partial z^2} - \frac{\partial^2\psi}{\partial x^2}\right)\right] = \mathrm{Rq}\left(1 + \sum_{k=1}^{2} P_k \frac{\mathrm{d}\Gamma_k}{\mathrm{d}\pi_k}\right)\frac{\partial T}{\partial x}, \tag{12}$$

where the phase buoyancy parameter P_k is given by

$$P_k = \frac{\mathrm{Rb}_k}{\mathrm{Rq}}\gamma_k' \tag{13}$$

and

$$\mathrm{Rb}_k = \frac{g h^3 \rho_0}{\kappa \eta_0} f_{ak}. \tag{14}$$

The density jumps are non-dimensionalized by division by ρ_0 and given in Table 3. Eq. (12) describes also the buoyancy of the thermally induced distortion of the phase boundaries.

For model calculations which aim at the Earth's evolution as a whole, it is vindicable that localized heat sources are neglected. Unlike the buoyancy effect of the thermally induced distortion of the phase boundaries, the latent heat as well as the heating by adiabatic compression and the frictional heating are omitted. Christensen and Yuen (1984, 1985) proved that the latter three effects vanish for vanishing dissipation number Di and that these effects are very small for earth-like Rayleigh numbers. The dissipation number is defined by

$$\mathrm{Di} = g\alpha h/c_p \qquad [\mathrm{D}]. \tag{15}$$

Neglecting all non-Boussinesq effects, the *conservation of energy* equation is

$$\frac{\partial T}{\partial t} + \frac{\partial\psi}{\partial z}\frac{\partial T}{\partial x} - \frac{\partial\psi}{\partial x}\frac{\partial T}{\partial z} = \frac{\partial^2 T}{\partial x^2} + \frac{\partial^2 T}{\partial z^2} + H(x,z,t), \tag{16}$$

where the non-dimensional specific heat production H is to be calculated from the non-dimensional variant of Eq. (1). Due to chemical fractionation, the abundances $a_{\mu\nu}$ of the radionuclide ν are functions of x, z and t. Therefore and because of the decay formula, the specific heat production is inhomogeneous and time-dependent. In our model K1 we used Eq. (17) in order to take into account the dependence of the viscosity on the dimensional temperature T_{dim} and, indirectly, on the pressure p_{dim}.

$$\eta = k_1 \exp(k_2 T_{\mathrm{m}}/T_{\mathrm{dim}}) \qquad [\mathrm{D}], \tag{17}$$

where k_1 and k_2 are constants. The melting temperature T_{m} is a given function of the depth. It is put together using the melting curve of olivine according to Ito and Takahashi (1987) for the upper mantle and the melting curve of perovskite according to Heinz and Jeanloz (1987) and Knittle and Jeanloz (1989) for the lower mantle. Some authors called the latter two papers in question. Therefore, we replace Eq. (17) by

$$\eta_\lambda = \eta_{0\lambda}\exp\left(\frac{E_0 + V_0 p_{\mathrm{dim}}}{R T_{\mathrm{dim}}}\right) \qquad [\mathrm{D}] \tag{18}$$

in this paper (model K2A). The quantities are explained in Table 3. E_0 and V_0 are taken from Riedel and Karato (1997). The dimensional pressure p_{dim} stems from PREM (Dziewonski and Anderson, 1981). For simplicity, we assume a unified formula for the mantle. There are only two exceptions: first, because of the high share of garnet in the transition layer the factor $\eta_{0\lambda}$ is estimated to be higher than in the main part of the mantle; second, we presume a constant lithospheric viscosity. The numerical values are listed in Table 3. All runs used in this paper have a 51×51 grid with 401×401 tracers. The maxi-

mum initial disturbance is 30 K. A small disturbance $T_s(x,z)$ is superimposed on the initial temperature to set the flow in motion. It is computed using

$$T_s(x,z) = A_s \sin\left(\frac{\pi x}{x_{max}}\right)\cos\left(\frac{\pi z}{2 z_{max}}\right) \qquad [D] \quad (19)$$

where A_s is the maximum initial disturbance. We assume neither very high temperatures nor very low ones but medium values as an initial temperature distribution for the evolution of the Earth using the evaluation by Stacey (1992) (p. 459). More detailed arguments for this assumption are given by Walzer and Hendel (1997a) (Section 2.4). As in K1 the parameter k_8 is 5.55. The upper and the lower limits of the viscosity are fixed at $10^{\pm 4} \cdot \eta_0$ Pa s.

2.2. Lithosphere

Here, some details are communicated. They serve to make the algorithm understandable and reconstructible.

A realistic lithospheric rheology with respect to very slow rock creep should be different from the corresponding rheology of the rest of the mantle. Presumably, different constitutive laws would be appropriate for the different layers which form the CC and the oceanic crust, the continental mantle lithosphere and the oceanic one. We suppose that the different creeping behaviour cannot be accurately described by a uniform constitutive equation distinguishing the layers only by different parameters. That is just the procedure of all published convection models and of the present paper, too. For that reason, it is up to now impossible to model the subduction of the oceanic slab in a physically comprehensive way. We assume some artificial features for the lithosphere, too, since we take a particular interest in the thermal and chemical mantle evolution as a whole. The prepared mechanism is as follows: The lithosphere is a layer under the surface with a depth $D_c = 100$ km. The fluid mechanics represented in Section 2 is applicable up to the surface. However, the temperature and pressure dependence of the viscosity, Eq. (18), does not apply in the D_c layer but the lithospheric viscosity is a constant value of 5×10^{22} Pa s. The heat sources are represented by tracers, the inflow into the lithosphere and the outflow out of the lithosphere of which is permitted only at certain places, the spreading zones and the subduction zones, respectively. Fig. 1 shows the exceptional movement of the *tracers* in the spreading zone, Fig. 2 in the subduction zone, respectively. However, all conservation laws are fulfilled also in these small regions. Elsewhere, the tracers are dragged by the solid-state flow. This rule is broken only by the chemical differentiation connected with the OIB volcanism or with the generation of oceanic plateaus. The observed hot spots are not systemati-

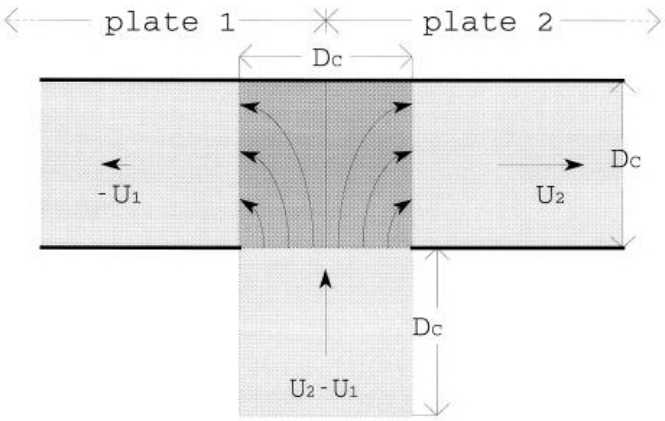

Fig. 1. Schematic representation of a spreading zone.

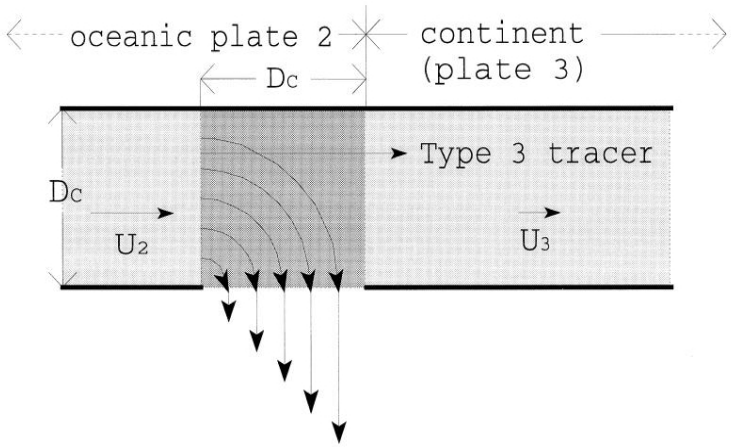

Fig. 2. Schematic representation of a subduction zone on the left margin of the continent.

cally related to the positions of the observed spreading axes and subduction zones. In the beginning, the model lithosphere is only *one* oceanic plate. As the whole primordial mantle rectangle, it is filled with Type 1 tracers only. After that, Type 3 tracers come into being in this lithosphere. The developing mechanism of these Type 3 tracers is explained in the paragraph superscribed with *Chemical differentiation*. In the D_c layer, *all* tracers move with the same only horizontal velocity U_0 as long as no continent came into being. This U_0 is computed by working out the average of the horizontal component u of the creeping velocity over all grid points in a $2D_c$ thick layer under the surface. This prescription is induced by the idea that the parts of the mantle near to the surface move like a plate and that the plate is driven by the vector sum of the forces caused by the asthenospheric convection. The Type 3 tracers have been defined as enriched in incompatible elements. The model continent is produced where two Type 3 tracers are neighbours in such a way that there is no non-Type 3 tracer closer to one of the Type 3 tracers than the distance between both Type 3 tracers. Additionally, the distance between the two Type 3 tracers must be smaller than the regular x distance of neighbouring tracers at the beginning of the run. Because of the periodic boundary conditions, the randomness of the location of the initial continent production is no restriction. The Type 3 tracer which is situated extremely far to the left (right) defines the left (right) margin of the continent, also later when the continent has grown. Because of the periodic boundary conditions, the aspect-ratio-three rectangle representing the mantle can be thought to be bended to a cylinder jacket. In the beginning, the spreading zone is installed just opposite to the initial continent. After that, however, the spreading zone can move without restrictions according to the dynamics. So, the location of the spreading zone is fixed arbitrarily only in the beginning. The spreading zone divides the oceanic lithosphere in a plate 1 and a plate 2. The continental plate has the index 3. The three plates consisting of tracers move with horizontal velocities U_1, U_2 and U_3. Within one plate the velocity is uniform. If the direction of it is to the right it is taken to be positive. The velocity U_k (where $k = 1, 2, 3$) is computed by working out the average of u over all grid points in a $2D_c$ thick layer under the surface confined to the (moving) section of plate k. Since the velocities U_1, U_2 and U_3 have in general different magnitudes it must be defined what happens at the sutures of the plates. The prescribed movements of the tracers in the spreading zone is depicted in Fig. 1. In the main part of the oceanic plate 2, that is plate 2 without spreading zone, the tracers move with a velocity U_2 to the right. In the main part of the oceanic plate 1 they move with $-U_1$ to the left. In the square beneath the dark-gray spreading square, all tracers rise with the magnitude of $U_2 - U_1$. In the spreading square, the tracers move along the quarter of an

ellipse to the right or to the left. The tracers are not permitted to cross the bold lines of Fig. 1. The viscosity of the spreading square is set to be equal to the lowest viscosity value in the oceanic asthenosphere. The lower boundary of the asthenosphere is in 410 km of depth. In the present model only *one* continent is permitted, the plate 3. The following items suggest themselves: if $(U_2 - U_3) \geq 0$ then the subduction zone is on the left margin of the continent. If $(U_3 - U_1) \geq 0$ then the subduction zone is on the right margin of the continent. If there is a transfer from one inequality to the other one in the course of a run, the subduction zone obviously changes the margin. Fig. 2 shows a subduction zone on the left continental margin. Moving through the dark-gray subduction square, Type 3 tracers flow into the continent with a velocity U_2, whereas the other tracers quit their previous horizontal velocity U_2 and move into the asthenosphere again where the creeping velocity carries the tracers as usual. The inflow of Type 3 tracers into plate 3 outlines roughly the continent growth by accretion of oceanic plateaus. If such a Type 3 tracer coming from the oceanic lithosphere approached to a continental Type 3 tracer letting an initial tracer distance between them then it will be a continental Type 3 tracer, too, than means in future it moves with the continent velocity U_3. By this procedure the continent has grown and the left margin of the continent is newly defined by that. If the entering Type 3 tracer did not meet at a *continental* Type 3 tracer in the deeper parts of the continent then it laterally penetrates to a distance D_c at the most and moves from now on with the continental velocity U_3. The viscosity of the subduction square is equal to the lowest viscosity of those grid points which are situated in the oceanic asthenosphere, too. Likewise the tracers may not cross the bold lines of Fig. 2. For the left margin of the continent, we assume: if $(U_2 - U_3) < 0$ then, henceforth, the plates 2 and 3 have a common velocity which is determined by working out the mean of the u values commonly for the segments 1 and 3. However, the common velocity is designated U_3. In this case, U_3 is the velocity of a plate containing both continent and ocean. For the right margin of the continent it applies that if $(U_3 - U_1) < 0$ then hereafter the plates 1 and 3 have a common velocity which is received by working out the mean of the u values for the segments 1 and 3. This common velocity is called U_3, too. For the spreading zone we have: if $(U_2 - U_1) \geq 0$ then from now on the spreading zone moves with a velocity $(U_2 + U_1)/2$. If $(U_2 - U_1) < 0$ then, henceforward, the plates 1 and 2 move commonly. The concerted velocity is found by working out the mean of the u values of the segment 1 and 2. Its designation is U_2. It is obvious that in this case at this place the spreading mechanism is temporarily suspended.

2.3. Chemical differentiation

In the beginning of a run, the 401×401 tracers are distributed regularly on the x–z plane. The tracers are trailed with the starting convection currents by which the initially regular distribution is destroyed. In the real Earth the nearest approach of the actual temperature to the melting temperature will happen in the asthenosphere, that is, in 100 to 410 km depth. Therefore, the chemical segregation causing the development of the oceanic plateaus is expected to take place in the asthenosphere. For that reason we presume the evolution of partial melt in the asthenosphere if the temperature-dependent viscosity drops below a threshold value $\eta_{\mathrm{th}\tau} = 2.1 \times 10^{20}$ Pa s in a sufficiently large area where the rising melt carries up a lot of U, Th and K. In comparison with solid-state convection it happens virtually instantaneously. Therefore, we model this process as follows. The source region in the asthenosphere is left depleted, that is, the Type 1 tracers are replaced by the depleted Type 4 tracers (see Table 2) in that region. As a compensation, a lithospheric Type 1 tracer must be transformed into a Type 3 tracer. The original lithospheric tracer had abundances of $k_8 a_{\mu\nu}^{(1)}$ for $\nu = 1, 2, 3, 4$ (see Table 1). After the fractionation it has the higher abundances, $a_{\mu\nu}^{(3)}$. The difference $a_{\mu\nu}^{(3)} - k_8 a_{\mu\nu}^{(1)}$ must be compensated by the transformation of $(z_{\mu\nu}^*)$ Type 1 tracers in the source region. One source region tracer had originally the abundances, $k_8 a_{\mu\nu}^{(1)}$. It has been transformed into a Type 4 tracer with the lower abundances, $a_{\mu\nu}^{(4)}$. That is why the number of Type 1 tracers, $z_{\mu\nu}^*$, that is necessary to generate one Type 3 tracer (enriched in radiogenic isotopes) is defined by

$$a_{\mu\nu}^{(3)} - k_8 a_{\mu\nu}^{(1)} = (z_{\mu\nu})^* \left(k_8 a_{\mu\nu}^{(1)} - a_{\mu\nu}^{(4)} \right) \qquad (20)$$

This equation ensures the conservation of the numbers of parent and daughter nuclei during the chemical fractionation. Since the tracers are indivisible, we use additionally

$$z_{\mu\nu} = \mathrm{round}(z^*_{\mu\nu}). \tag{21}$$

Some details of the code are described now. If a tracer is situated in the surrounding rectangle of a grid point, then we christen the latter one the associated grid point. If at the associated grid point of a Type 1 tracer the relation $\eta(T) < \eta_{\mathrm{thr}}$ applies, then this tracer is designated as a *Type 1 tracer with* $\eta < \eta_{\mathrm{thr}}$. For each time increment, a rectangle of *minimum* height h_τ is formed around each Type 1 tracer with $\eta < \eta_{\mathrm{thr}}$. The ratio a_τ of width to height, h_τ, of the rectangle is fixed, $a_\tau = 2$. The reference tracer is located in the centre of the rectangle. The following applies in the rectangle including the boundary: {It contains exactly $z_{\mu 4}$ Type 1 tracers with $\eta < \eta_{\mathrm{thr}}$ for $k_8 = 1$ in the aforementioned formula and *these* Type 1 tracers represent more than 50% of the tracers in the rectangle.} If no h_τ can be found, we set $h_\tau = 10^{40}$ for a technical reason. For each time increment, the following will now be performed: For all h_τ satisfying $h_\tau < 10^{40}$, the lowermost value is selected. Let this value be $h_{\tau,\min}$. If there is no $h_{\tau,\min}$, we proceed to the next time increment. Otherwise: {All Type 1 tracers with $\eta < \eta_{\mathrm{thr}}$ lying in and on the rectangle with $h_{\tau,\min}$ are suddenly transformed into Type 4 tracers. The centre of gravity of the tracers to be transformed is projected perpendicularly onto the surface. Let this point be designated as P'. The $rz_{\mu\nu}$ Type 1 tracers *in* the D_c layer situated next to P' are transformed into Type 3 tracers where

$$rz^*_{\mu\nu} = \frac{1\left(a^{(3)}_{\mu\nu} - a^{(1)}_{\mu\nu}\right)\left(k_8 a^{(1)}_{\mu\nu} - a^{(4)}_{\mu\nu}\right)}{6\left(a^{(1)}_{\mu\nu} - a^{(4)}_{\mu\nu}\right)\left(a^{(3)}_{\mu\nu} - k_8 a^{(1)}_{\mu\nu}\right)} \tag{22}$$

and

$$rz_{\mu\nu} = \mathrm{round}(rz^*_{\mu\nu}) \tag{23}$$

where $rz_{\mu\nu}$ is the number of the new Type 3 tracers.} The non-dimensional stream function ψ is confined to values between 0 and 10^6, the dimensional temperature lies between 0 and 8000 K. This does not mean that these values are obtained in the runs, but they are the cutting values in the code.

2.4. Local marker refresh (LMR)

We developed an algorithm which prevents that the surrounding rectangle of a grid point will be empty of tracers. In this case the heat production density would be undetermined. The construction of the LMR algorithm guarantees the constancy of the number of parent plus daughter atoms of each decay series. We apply the algorithm to surrounding rectangles, the number of tracers of which have become less than 50% of the average marker number per surrounding rectangle. We relocate tracers of the four neighbouring surrounding rectangles having common sides with the rectangle of the diminished marker number into the latter destination rectangle. This relocation fulfills six conditions: First, the total number of tracers of each type in the computational area is conserved exactly during the LMR procedure. Second, the final numbers of tracers in the origin surrounding rectangles and in the destination rectangle should be as equal as possible. Third, the ratios of the number of Type i tracers to the number of Type j tracers in the origin rectangles should have a minimum alteration for each rectangle and for i, $j = 1, 3, 4$ with $i \neq j$. Fourth, the shift of a tracer is taken to be one grid point distance in the corresponding direction. Fifth, the LMR is executed *separately* for the lithosphere and rest of the mantle, that is, surrounding rectangles containing the bold lines between the lithosphere and the rest of the mantle (cf. Figs. 1 and 2) are not included in the LMR. However, the lower sides of the spreading and subduction squares are included. The periodic boundary conditions are taken into account, that is, for the right (left) margin the surrounding rectangles of the left (right) margin are taken to be the right (left) neighbours. Sixth, Type 3 tracers are excepted from LMR. Their existence influences the result only indirectly by the third rule.

2.5. A comparison between our model K1 and this paper (K2A)

The present new model, K2A, describes the thermal and chemical evolution of the Earth's mantle and crust, too. It differs, however, from our previous model K1 by several items. Walzer and Hendel (1997a) outline the essential features of the calculation of K1 and the problem of the initial conditions

that depends on the assumptions made regarding the accretion mechanism of the Earth. Walzer and Hendel (1997b), however, draw conclusions from K1 regarding geotectonics, magmatism and other Wilson cycle phenomena. Here, the distinguishing features of K1 and K2A are specified.

In K1, no phase transitions have been taken into consideration. No pre-K1 run with whole-mantle convection made it possible to receive *all* known observational facts and numbers simultaneously from one run. Therefore we presumed heuristically $w = 0$ at 660 km depth, that means that no material is permitted to flow across that discontinuity. Although entirely excellent results have been calculated using that assumption, that supposition is somewhat artificial from the physical point of view. So, in the case of K1, the double-layer convection is prescribed. In this paper, however, we drop that artificial assumption. We did not introduce any compulsory conditions for the interior of the box, neither for the velocity nor for any other quantity. Instead of it we introduced the two phase transitions at 410 and 660 km depth in a physical way using accepted values of the Clapeyron slope γ_k, the excess pressure π_k and the density contrast. In the case of K2A, we *obtained* a leaky double-layer convection *as a result* and we *received* a depleted upper part of the mantle and an enriched lower part of the mantle *as a result* for the present time. For details see Section 3.

A further big difference between the models is that in K1 the Type 3 tracers stay simply randomly distributed in the lithosphere. Clusters of them are produced only by the chemical fractionation. The parts of the lithosphere enriched in incompatible elements do not cluster to continents with dense accumulations of the enriched Type 3 tracers. In the case of K2A, however, the enriched parts of the lithosphere are collected by continental accretion. The simplified mechanism of it has been described in the paragraph entitled with *Lithosphere*.

Further differences concern the boundary conditions. In the case of K1, the conditions $\partial T/\partial x = 0$, $\psi = 0$ and $\nabla^2\psi = 0$ are prescribed for the sidewalls whereas periodic boundary conditions are introduced in K2A. Regarding the boundary conditions on top, only the temperature was adapted to the observed annual average of the present (Mitchell, 1989). So, instead of $T_{\mathrm{dim}} = 300$ K, $\psi = 0$ and $\nabla^2\psi = 0$ for K1 we introduced $T_{\mathrm{dim}} = 288$ K, $\psi = 0$ and $\nabla^2\psi = 0$ for the new model. For the bottom, a vanishing heat flow, $\psi = 0$ and $\nabla^2\psi = 0$ have been presupposed in the case of K1 whereas $q_{\mathrm{CMB}} = 20$ mW m^{-2}, $\psi = 0$ and $\nabla^2\psi = 0$ apply for K2A taking into account results on the driving mechanism of the dynamo (cf. Appendix A).

For K1, the temperature dependence of the viscosity is given by $\eta = k_1 \exp(k_2 T_{\mathrm{m}}/T)$ where T_{m}, the melting temperature of olivine by Ito and Takahashi (1987), is taken for the upper mantle and that of perovskite by Heinz and Jeanloz (1987) and Knittle and Jeanloz (1989) is adopted for the lower mantle. Here, the pressure dependence of the viscosity is hidden in T_{m}. For K2A, on the other hand, we used a viscosity $\eta_\lambda = \eta_{0\lambda} \exp[(E_0 + V_0 p_{\mathrm{dim}})/RT_{\mathrm{dim}}]$. For K1, the constant k_1 is uniform in the whole mantle whereas in the case of the new model we used an elevated $\eta_{0\lambda}$ value for the transition layer in order to describe the influence of its high percentage of garnet, however, in the rest of the mantle (without lithosphere) $\eta_{0\lambda}$ is taken to be constant, too.

In K1 we did not use a *Local Marker Refresh*, whereas in this paper is was introduced. It is described above in the corresponding paragraph. In both models we assumed moderate initial temperature distributions T_{anf} of the evolution model. In K1 we took $T_{\mathrm{anf}} = 0.71 T_{\mathrm{m}}$. For K2A we interpreted the temperature distribution by Stacey (1992) (p. 459) as initial temperature curve.

3. Results

3.1. Geophysical and geological results

The model K2A has been described in Section 2. We made a lot of runs of it varying the Rayleigh

Fig. 3. In the upper panel, the evolution of the horizontally averaged heat flow q_{ob} is depicted. The second panel shows the number of newly generated Type 3 tracers per 25 Ma. It is a measure of the potential juvenile continent growth as a function of time. The third panel shows the evolution of the lateral velocity of the continent. The lower panel gives the vertical mass flux function F as a function of time.

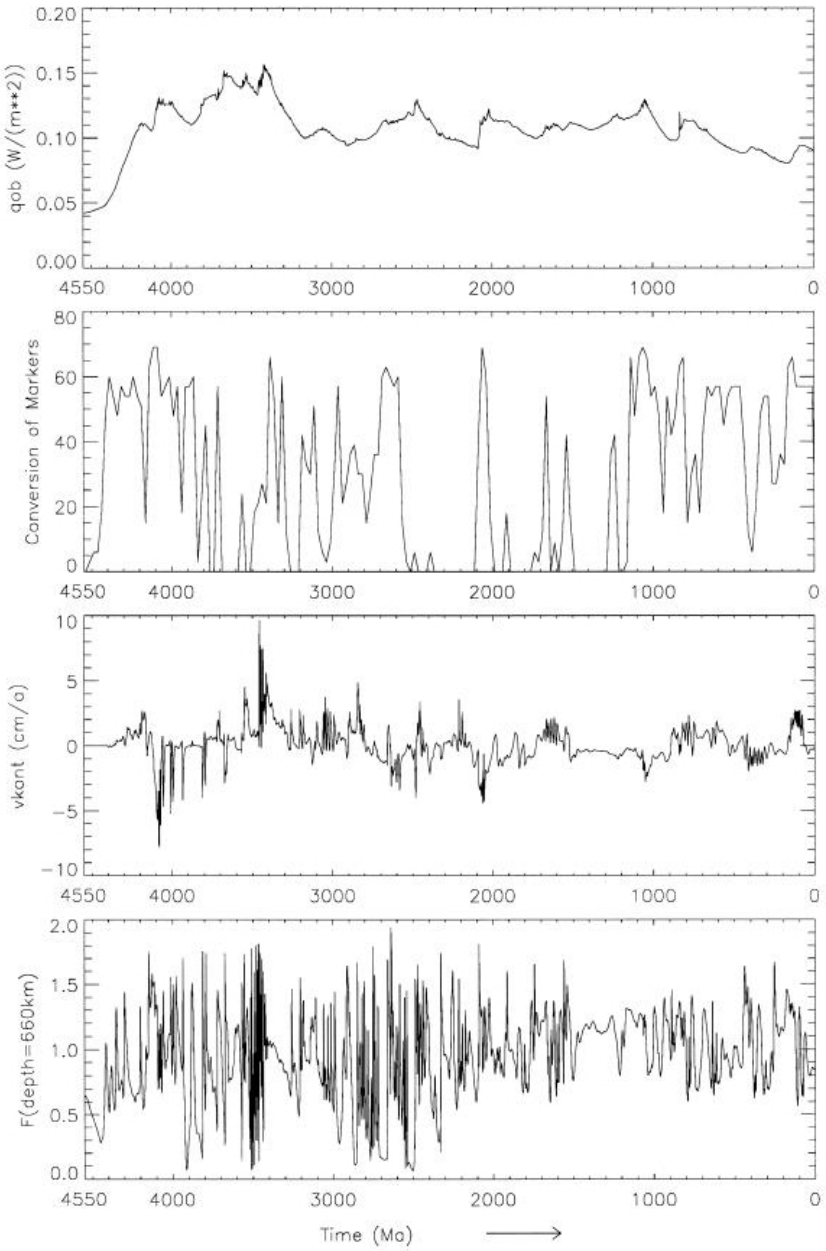
qob (W/(m**2))
0.20
0.15
0.10
0.05
0.00
Conversion of Markers
80
60
40
20
0
vkant (cm/a)
10
5
0
−5
−10
F(depth=660km)
2.0
1.5
1.0
0.5
0.0
4550
4000
3000
2000
1000
0
Time (Ma)

number, Rq, between 1.4×10^6 and 1.0×10^9 using a finite difference scheme. Before the discussion of the wealth of data, we want to present the results for $Rq = 1.5 \times 10^6$. A slow decline of the mean surface heat flow from the Archean to the Proterozoic and to the Phanerozoic has been concluded by Pollack (1980, 1986) and Nyblade and Pollack (1993). A similar tendency is perceptible in the first panel of Fig. 3 which shows the laterally averaged model surface heat flow, q_{ob}, as a function of time. Using 24 774 observations from heat flow measurements, Pollack et al. (1993) calculated a mean global heat flow of 87 mW m^{-2} for the present. The mean heat flow of the oceanic bottom is 101 mW m^{-2}. The final value of the model heat flow, q_{ob}, is nearly equal to the observed 87 mW m^{-2}.

The increase in really new mass of the continent has been computed and is depicted in the second panel of Fig. 3. This curve must be compared with the augmentation of the *total* mass of all continents and oceanic plateaus. It means, not every accretion of terranes to a continent is a matter of importance for this quantity but only the accretion of juvenile parts which came from the mantle. The CC is derived by partial melting in the asthenosphere and forms the complementary reservoir of the depleted mantle (Hofmann, 1988). Naturally, we want to discuss only the general course of the curve of conversion of markers and not each peak since these peaks are stable only for minor variations of Rq. Nevertheless it can be expected that periods of augmented tectonic activity can be explained in principle by a similar mechanism. However, here we discuss only the general course since it is stable for a stronger variation of the Rayleigh number, Rq. Only a few workers advocate the opinion, yet, that nearly the whole volume of the CC differentiated immediately at the beginning of the Earth's evolution, e.g., Armstrong (1991). Today we can state a growing consensus that the CC grows episodically over billions of years (Taylor and McLennan, 1995). At least 60% of the present CC have been produced by the late Archean according to the quoted authors. O'Nions et al. (1979) arrive at the conclusion that the quantity concerned is less than 60%, according to Allègre (1982), it is about 60%. Rudnick (1995) concluded from a diversity of Sm–Nd studies that 35–60% of the present continental mass was formed in the Archean. A value of 50% is concluded for an age of 2500 Ma from the mass ratio vs. time curve of Kramers and Tolstikhin (1997). Of course, the quoted values have a certain error bar so that the about 50% which can be received by integration over our curve for the conversion of markers (Fig. 3, second panel) is a good result. There are, however, divergent opinions on the problem of the prevailing mechanism of the episodic accretion of new mass batches to the continent. Taylor and McLennan (1995) presume an andesitic composition of an averaged CC. They suggest that the continents grow mainly by accretion of island arcs of andesitic composition. The granites and granodiorites of the Proterozoic and Phanerozoic upper CC evolve by further chemical fractionations whereas in the Archean tonalites, trondhjemites and granodiorites develop instead of them. The latter rocks are strongly enriched in incompatible elements, too. Abbott et al. (1997) are convinced, on the contrary, that the continents grow by addition of oceanic plateaus, hotspot tracks and, to a minor degree, island arcs. So, they emphasize that island arcs do not have the average composition of the CC whereas volcanic material from the Ontong Java and Manihiki and other oceanic plateaus have a basaltic composition with an enriched amount of incompatible elements and enough Cr and Ni which reproduces the average composition of the CC. Oceanic crust with a thickness ≥ 27 km is unsubductible for ≥ 0.25 Ga. Examples are the present Ontong Java plateau and accreted terranes with hotspot characteristics from Vendian to Permian. The observed thickness of the Ontong Java plateau fits the hypothesis since it is at the lower boundary of the distribution of the observed continental thicknesses. It is evident that the oceanic plateau model is compatible with our model K2A, but not all details of it are necessary for K2A. Rudnick (1995) has a conciliatory standpoint between the island arc model and the oceanic plateau model. She pointed out that the trace-element

Fig. 4. The evolution of the temperature, T. The snapshots stand for the ages given at the upper left corner of each panel. The motion is dominated by thermally induced density differences. The grid consists of 51×51 elements. $Rq = 1.5 \times 10^6$.

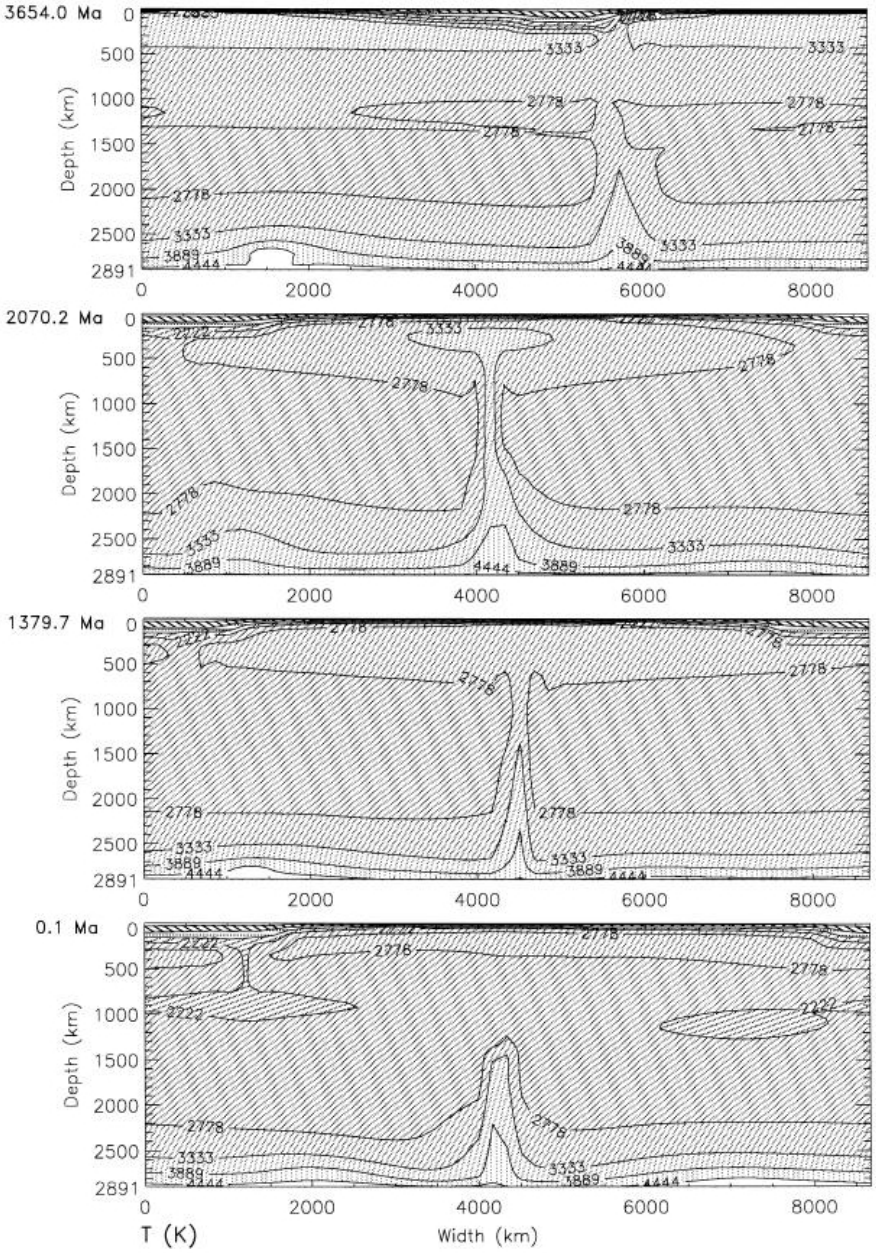
3654.0 Ma
2070.2 Ma
1379.7 Ma
0.1 Ma
Depth (km)
0
500
1000
1500
2000
2500
2891
2222
2778
3333
3889
4444
0
2000
4000
6000
8000
T (K)
Width (km)

distribution of the CC can be explained by growth through a mixture of convergent margin and intraplate magmatism. Our model cannot reflect the discussed details of the accretion models since the gridpoint distance is too large and the algorithm too simple, yet. Nevertheless, the gross time distribution of the juvenile part of continental accretion is reflected in the second panel of Fig. 3.

The third panel of Fig. 3 shows the variations of the lateral velocity, v_{cont}, of the model continent independent of its growing size. The probability of the accretion of free Type 3 tracers to the model continent grows with the absolute value of v_{cont}.

Like Steinbach and Yuen (1992), we calculated a vertical mass flux function, F, as a function of time using

$$F = \frac{\left[a^{-1}\int_0^a w^2(x,z)\,\mathrm{d}x\right]^{1/2}}{\left[a^{-1}\int_0^a\left[\int_0^1\left(u^2(x,z)+w^2(x,z)\right)\mathrm{d}z\right]\mathrm{d}x\right]^{1/2}} \tag{24}$$

where a is the aspect ratio of the box. For a depth of 660 km, the quantity F is plotted in the fourth panel of Fig. 3 as a function of time.

The evolution of the temperature field is demonstrated by the four panels of Fig. 4. The age the snapshot is standing for is indicated at each upper left corner of the corresponding panel. The hot material can spread in the asthenosphere because the rising diapirs can occasionally break through the transition layer. Boehler (1996) concluded from new melting data on iron and from the decrease of the eutectic melting depression in the Fe–FeO–FeS system with increasing pressure that the temperature at the inner-core boundary is slightly less than 5000 K. The resulting temperature at the bottom of the mantle is about 4000 K. Boehler estimates a temperature decline of 1500 K for the lowermost parts of the mantle. The fourth panel of our Fig. 4 representing the present shows a laterally averaged temperature of about 4400 K at the CMB and a steep temperature decline of 1500 K across the lowermost 500 km of the mantle.

The snapshots of Fig. 5 demonstrate the viscosity distribution in the mantle for the same epochs as the temperature snapshots of Fig. 4. In the upper parts of the panels, there is a slowly evolving low viscosity layer. For the present, it extends down to about 1000 km of depth. This depth can be fixed only roughly since the viscosity increase is low. A smaller viscosity maximum exists between 410 and 660 km depth, but it is not visible in *these* plots since the viscosity differences between neighbouring isolines are too large here. This smaller maximum reflects the elevated garnet percentage in the transition layer. In all runs of the present model in the mentioned Rayleigh number span, we received high viscosity values for the lower half of the lower mantle except for the D'' layer and the plume pipes. Also other modern models established such large viscosity contrasts: van den Berg and Yuen (1997) investigated the role of viscous heating in two-dimensional steady-state models with Newtonian and non-Newtonian rheology. Their viscosity contrasts reach up to five orders of magnitude. Discussing geochemical, seismic and geoid evidence, Phipps Morgan et al. (1995) propose that the asthenosphere is plume-fed. So, the asthenosphere is not only hotter than the overlying oceanic lithosphere but also hotter than the underlying transition layer. Phipps Morgan et al. (1995) estimate a viscosity contrast of five orders of magnitude between the maximum in the lower half of the lower mantle and the minimum in the oceanic asthenosphere. These assessments correspond with our calculated viscosity values of Fig. 5 and our temperature distribution of Fig. 4. However, models of the radial profile of mantle viscosity, which have been derived from a simultaneous fit of long-wavelength free-air gravity harmonics and decay times estimated from the postglacial uplift, resulted in a similar profile but the contrast between maximum and minimum viscosity is only two orders of magnitude (Mitrovica and Forte, 1997). It is evident that the resolving power for the lower half of the mantle is considerably less than that for the upper half.

Fig. 5. A series of snapshots of the shear viscosity distribution in the mantle. The isolines are drawn for the logarithm of the viscosity expressed in Pa s. The ages are marked at the upper left corner of each panel.

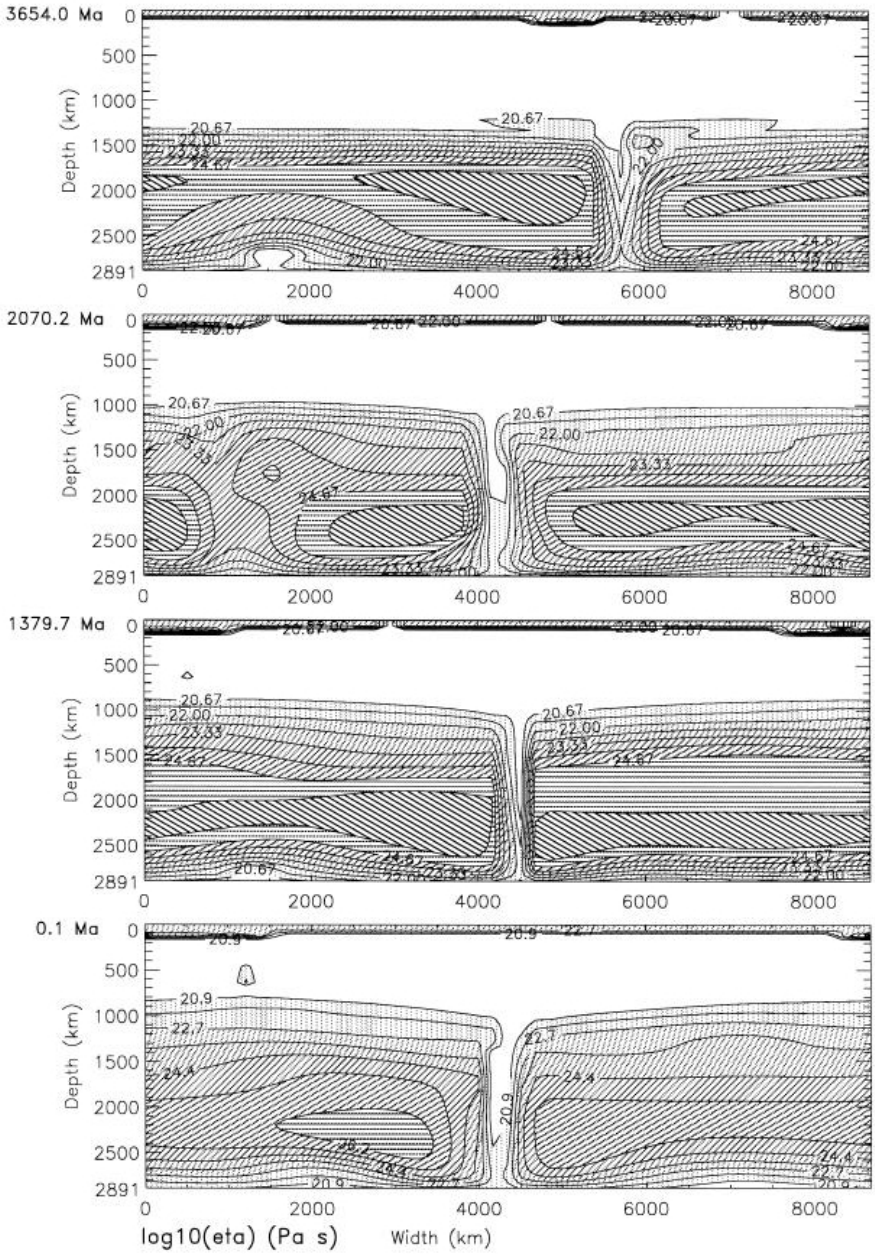
3654.0 Ma
2070.2 Ma
1379.7 Ma
0.1 Ma
Depth (km)
0
500
1000
1500
2000
2500
2891
0
2000
4000
6000
8000
20.67
22.00
23.33
24.67
20.9
22.7
24.4
log10(eta) (Pa s)
Width (km)

We received the interesting result that, compared with the lateral velocity of the continent, the hotspot pipes move only very sluggishly in the lower part of the lower mantle. This result applies for all runs made the Rayleigh numbers, Rq, of which varied from 1.4×10^6 to 1.0×10^9. Narrow upwelling plumes are maintained for a long period of time. If sometimes two model plumes emerge then, for a short time span like 120 Ma, they remain virtually fixed with respect to each other. This finding corresponds to the observation (Richards, 1991) that in the past 120 Ma there is no ascertainable relative motion between the hotspots in the Atlantic Ocean and in the Indian Ocean. So, the hot spots practically form a fixed reference frame relative to the moving plates. It is an incidental natural result of our model. In a lot of other convection models the position of the plumes is artificially fixed. Moreover, the position of our model plumes is not systematically related to the model plate boundaries. This fact corresponds to the observation. In the model, the plumes carry upward enriched tracers whereas in the real Earth the hotspot basalts are enriched in trace elements, enriched in comparison with MORB. Furthermore, in the real Earth there are ridge crossings by hot spot tracks. Therefore the hotspot source region must lie beneath the MORB source region. The model fulfils that expectation, too. We think that no pure whole-mantle convection model can be consistent with all the observations specified above.

A further remark is aimed at the globe encircling Dupal anomaly (Dupré and Allègre, 1983) that is situated between the equator and 60°S (Hart, 1984). It is related to a very early (> 3000 Ma) development of U/Pb, Rb/Sr and Th/U enrichments. In other words, the mass ratio $^{207}Pb/^{204}Pb$ is drawn as ordinate vs. $^{206}Pb/^{204}Pb$ in a first plot. Furthermore, $^{87}Sr/^{86}Sr$ vs. $^{206}Pb/^{204}Pb$ is drawn in a second plot, and $^{208}Pb/^{204}Pb$ vs. $^{206}Pb/^{204}Pb$ in a third one, respectively. In all diagrams, a straight line rises from the left bottom to the right top if the data stem from non-Dupal MORB of the Pacific and the Atlantic Ocean. Dupal data are significantly higher than this line. The permanence of the position of the anomaly since more than 3000 Ma is hardly understandable in the case of an only moderate viscosity maximum in the lower mantle. We expect that it will be possible to understand the mechanism of the permanence of the Dupal anomaly in a convecting mantle by transferring our $\eta(T, p)$ function, the phase transition description, the chemical differentiation and other details of our model to the spherical-shell convection model of Baumgardner (1985, 1988). Of course, a very early partial injection of crustal material should be taken into consideration.

It has already been pointed out that the lower panel of Fig. 5 shows our model-mantle viscosity of the geological present. The low-viscosity pipe in the middle of the lower mantle represents a plume rising from the D'' layer. Both this panel and the corresponding curve of laterally averaged viscosity as a function of depth demonstrate that the strong increase of the viscosity powers from 20.9 to 22.7 is not in 660 km depth but in about 1000 km depth. In addition, the mentioned averaged $\eta(z)$ curve shows that the general low-viscosity layer stretching from the bottom of the lithosphere down to 1000 km of depth is interrupted by a smaller viscosity maximum between 410 and 660 km depth. These findings are in excellent coincidence with the inversion model of Kido and Čadek (1997), which is based on geoid anomalies. In contrast to our paper, they assume that the viscosity only depends on the depth. In order to exclude the disturbing influences of the continental lithospheric keels and of the subducting slabs, they took into account only the tomographic anomalies beneath those parts of the oceans which are sufficiently far from the slabs. They used the seismic tomography results of Fukao et al. (1992) [0–2900 km], of Zhou (1996) [0–1200 km] and of Zhang and Tanimoto (1991) [0–500 km] from a surface-wave analysis. For the latter two models, they complemented the results by those of Fukao et al. (1992) for the deeper parts of the mantle. Kido and Čadek (1997) computed step functions for the viscosity as a function of depth maximizing the correlation between the observed and the predicted geoid. As an inversion technique for the approximation to the

Fig. 6. The streamlines of a series of snapshots the ages of which are given at the upper left corner of each panel. Negative ψ values stand for clockwise flow, positive ψ values represent an anticlockwise flow. The units are given in $m^2\ s^{-1}$.

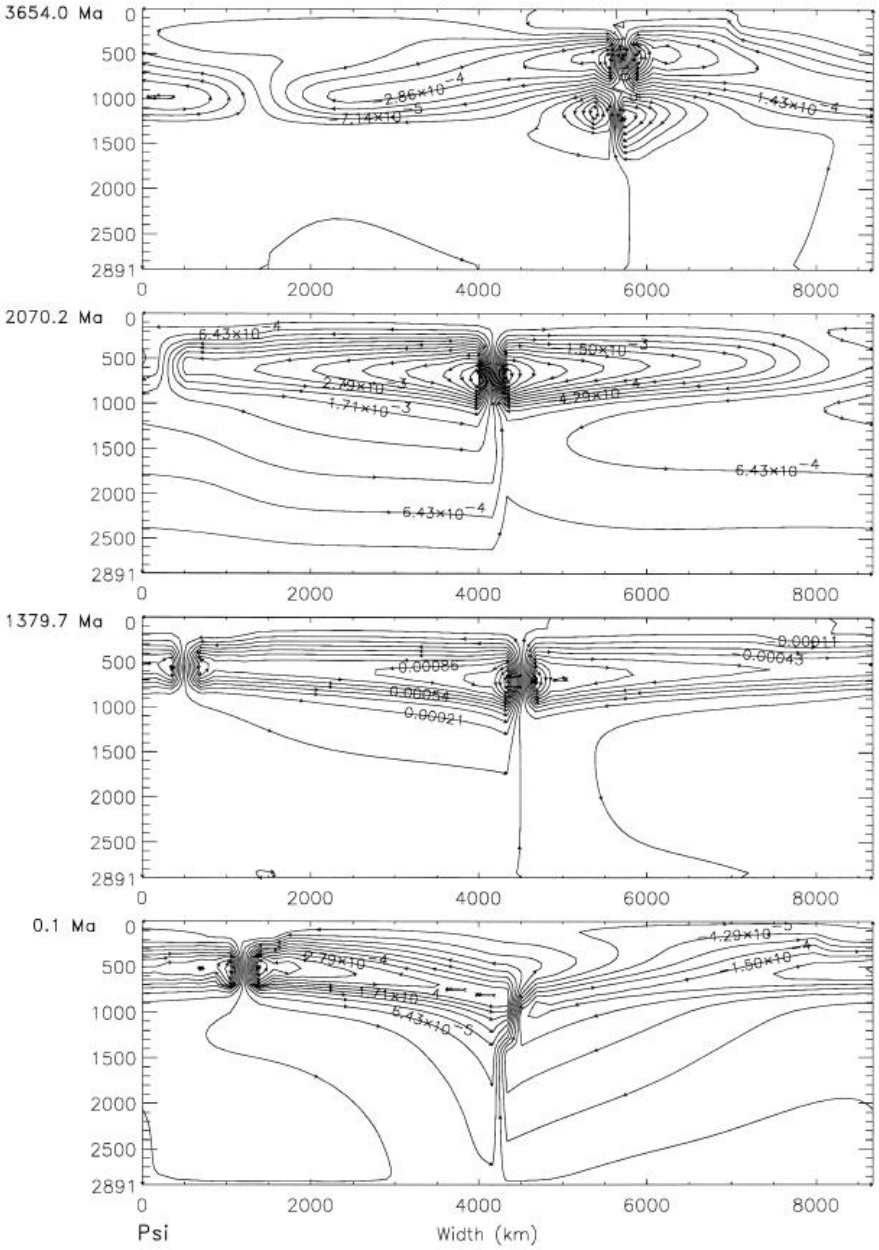
3654.0 Ma
2070.2 Ma
1379.7 Ma
0.1 Ma
0
500
1000
1500
2000
2500
2891
0
2000
4000
6000
8000
Psi
Width (km)

maximum value of the correlation coefficient they used the genetic algorithm that had been applied already by King (1995) to the problem. The viscosity distributions of Kido and Čadek (1997) have a great similarity among one another. This applies especially for the upper half of the mantle. Of course, the used intermediate-wavelength inversion ($l = 12$ to 25) is not sensitive to deep-mantle viscosity. Their principal result is that the main viscosity jump is in about 1000 km depth and not as usually stated in 660 km. Moreover their Fig. 6 shows a second low viscosity layer the thickness and the low viscosity values of which are in the same order of magnitude as those of the asthenosphere. Zhang and Christensen (1993) found that the long-wavelength geoid is in accord with the assumption of a low-viscosity zone below the 660-km seismic discontinuity. All these findings are in excellent agreement with the present model K2A (confer also Fig. 7).

Fig. 6 shows the evolution of the streamline distribution in the mantle. This picture is supplemented by the presentation of the absolute values of the creep velocity in Fig. 7. The sequence of the ages of the panels is the same for both figures. Clear indications of the influence of the smaller viscosity maximum in the transition layer is visible, especially obvious in Fig. 7. It was to be expected that the intermediate layer of elevated viscosity is bended upward in the downwelling current on account of the phase boundaries (cf. the upper panels of Figs. 6 and 7). In the reverse case, the downward bending of the thin higher viscosity layer is in the upwelling current (cf. the lowermost panels of Figs. 6 and 7). This intermediate layer of augmented viscosity cannot be distinguished in Fig. 5, because the viscosity difference of neighbouring isolines is too large.

3.2. Geochemical results

The following pictures (Figs. 8–10) deal with the evolution of the geochemical reservoirs and with the origin, the growth and the lateral migration of the continents. First of all the symbols of the plots are defined. They apply equally for all of these figures. Type 1 tracers are represented by small black dots. Type 4 tracers stand for the depleted mantle in the sense of the definition of residuum 1 of Hofmann (1988). The latter depleted tracers are not depicted by single symbols but their share in the tracers of a surrounding rectangle is pictured by different degrees of lightness of gray. All used degrees are to be seen, e.g., in Fig. 9e. In the following we define the degrees mentioned. For the whole mantle beneath the D_c layer under the surface, the share, A', of the Type 4 tracers is allocated to the surrounding rectangle of a grid point. We use $A' = i_4/(i_1 + i_4)$ where i_4 is the number of Type 4 tracers in the surrounding rectangle and i_1 is the number of Type 1 tracers, respectively. A smoothing of the representation has been introduced as follows. We start from a two-dimensional field A'. The indices of the grid points in the x direction and the z direction are denoted as i and j, respectively. The smoothing function changes the value $A'(i,j)$ at this grid point into $A(i,j)$ where

$$A(i,j) = \left[\sum_{k=i-2}^{i+2} \sum_{l=j-2}^{j+2} A'(k,l) \right] \Big/ 25. \qquad (25)$$

The periodic boundary conditions have been taken into account for the sidewalls. At the lower boundary the last but one row and the last but two row have been reflected at the CMB and taken into consideration for the smoothing. If $A \leq 0.3$ then the surrounding rectangle stays white. If $A > 0.3$, $A > 0.35$, $A > 0.40$, $A > 0.45$ or $A > 0.50$ then the rectangle is gray. The higher the A-limit is the darker is the gray. For the D_c layer the quantity i_3 is the number (per surrounding rectangle) of those Type 3 tracers which are connected to form the continent whereas i_{3op} is the respective number of Type 3 tracers which have not accreted to the continent, yet, and which therefore belong to the oceanic plateaus. We define $B' = i_3/(i_1 + i_3 + i_{3op} + i_4)$. Replacing A' and A by B' and B, respectively, in Eq. (25), we receive a smooth quantity, B. If $B > 0.5$ the area is left white. It represents the continent. Finally, we use $C' = i_{3op}/(i_1 + i_3 + i_{3op} + i_4)$. Replacing A' and A in Eq. (25) by C' and C, respectively, we get a new smooth

Fig. 7. Four snapshots of the absolute value of the creeping velocity of mantle rocks. The chosen ages are the same ones as in Figs. 4–6. Note the influence of the transition layer and its deformation by the flow.

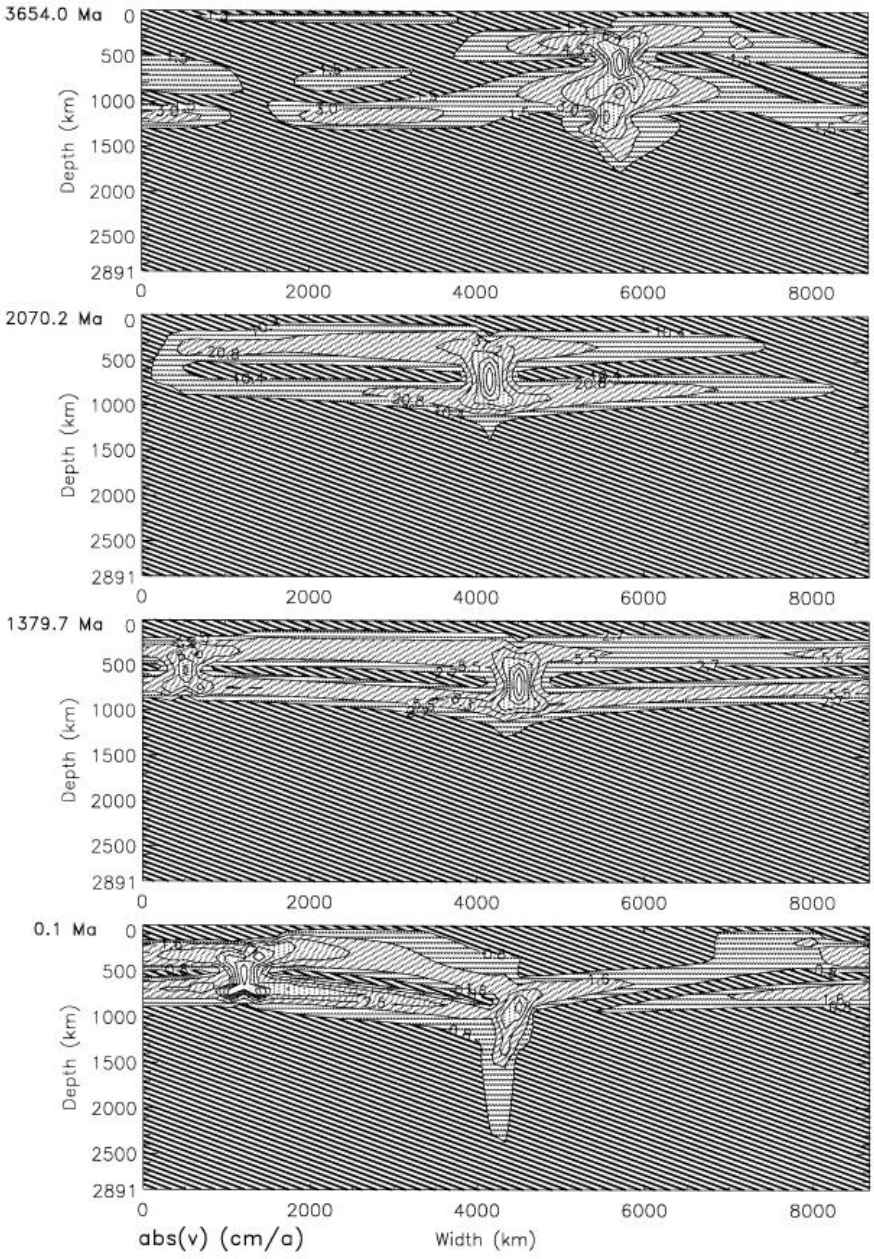
3654.0 Ma
2070.2 Ma
1379.7 Ma
0.1 Ma
Depth (km)
0
500
1000
1500
2000
2500
2891
0
2000
4000
6000
8000
abs(v) (cm/a)
Width (km)

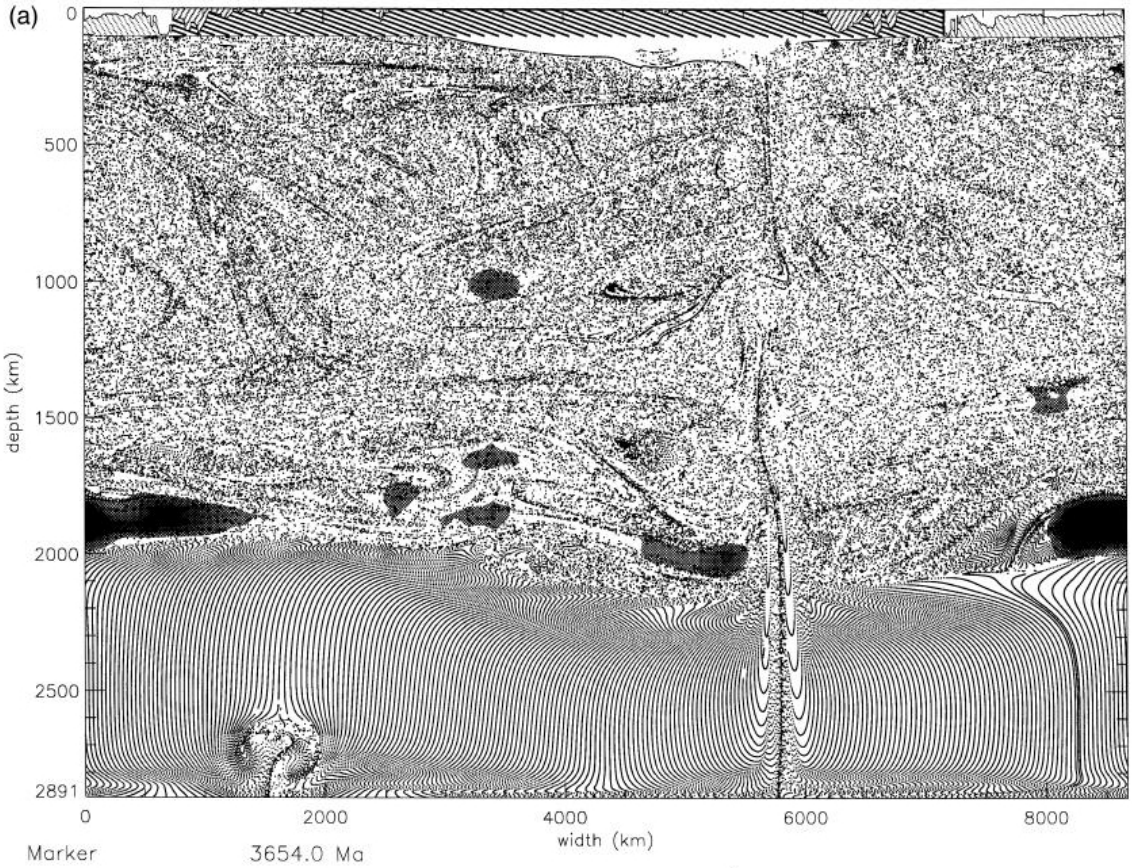

Fig. 8. The evolution of the geochemical reservoirs in the Archean and in the early Proterozoic for $Rq = 1.5 \times 10^6$. The snapshots stand for an age of 3654.0, 2070.2 and 1920.4 Ma. The denotation of signs and hatchings is explained in Section 3.2.

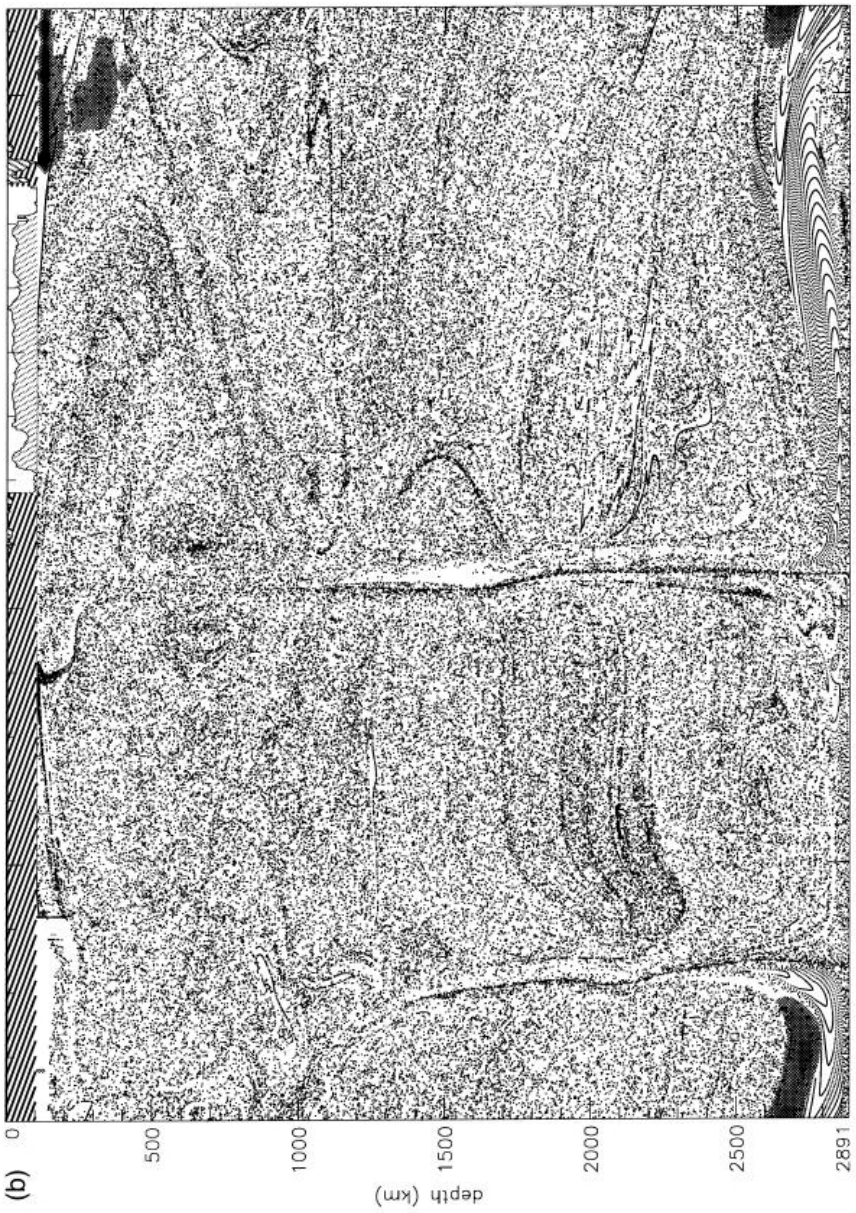

Fig. 8 (continued)

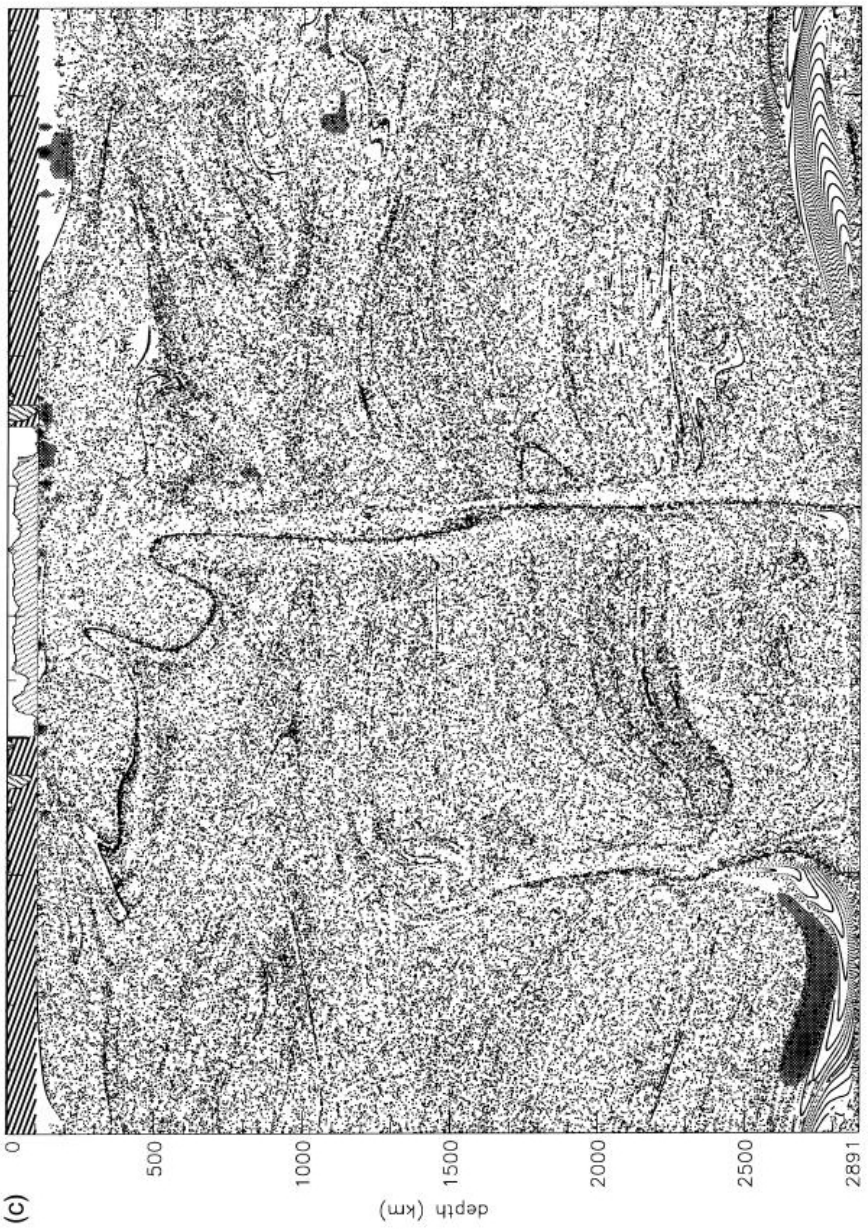

Fig. 8 (continued)

quantity, C, by which using $C > 0.5$ the oceanic plateaus are defined. These plateaus are depicted by an oblique hatching the lines of which run from a left-hand bottom to a right-hand top. However, the lithosphere with MORB is represented by a hatching with thick slanting lines from a left top to a right bottom.

We would like to emphasize that our model is based on thermal solid-state convection with inhomogeneous distributions of radiogenic heat sources. The redistribution is induced by chemical differentiation whereas the convective motions aim at rehomogenization, especially in areas where the viscosity permits a strong shearing flow, e.g., in the asthenosphere. The dependencies of the viscosity on pressure and temperature and the two phase boundaries in 410 and 660 km depth are essentials of the model K2A. As opposed to this, Dupeyrat et al. (1995) deal with the question of exclusively upper mantle convection of a binary eutectic material with *constant* viscosity assuming a rigid upper surface. In our model, the plate velocities have been calculated whereas Dupeyrat et al. (1995) *prescribe* a constant or even zero plate velocity. The model by Kameyama et al. (1996) seems to be more realistic. It is a further development of the paper of Ogawa (1994). It assumes upper mantle convection of a binary eutectic material and a Newtonian temperature-dependent rheology. The result of it is a chemically stratified upper-mantle structure which is possibly characteristic for the early Archean. However, our model is compatible with the result that the geochemical evidence against *gross* compositional layering of the mantle is conclusive (O'Neill and Palme, 1998) and that the near-chondritic Re/Os ratio of the upper mantle is an argument against the differentiation of the mantle by olivine flotation (O'Neill et al., 1995). Therefore, in this paper, the chemical differences of *mantle* reservoirs refer to the incompatible elements. Now we discuss the chemical evolution of the mantle and the crust for the moment, keeping the Rayleigh number constant ($Rq = 1.5 \times 10^6$) and taking into account the above remarks. For a certain surrounding of $Rq = 1.5 \times 10^6$ and for $2.0 \times 10^6 \leq Rq \leq 2.4 \times 10^6$, *all* model results are in between good and excellent correspondence with the geochemical and geophysical observations. It would be too much to present all these results here. Fig. 8a shows a snapshot for an age of 3654.0 Ma, for the Archean. The lower 900-km layer of the mantle is primordial, yet. It is nearly not influenced by the convective flow. On the right-hand side of it, a thermal plume breaks through it rising from the CMB. The plume does not ascent as far as the lithosphere. On the contrary, it has caused a strong stream that is directed downwards (cf. Fig. 6, upper panel). On the left-hand side at the CMB, a thermal plume is in its state of emergence. Unlike the present state the first depleted mantle areas are situated not in the upper mantle but in the lower mantle just above the primordial lower layer. The (white) continent did not arrive at its final size, yet. Oceanic plateaus are near the continental margins. They will approach to the continent by oceanic plate movement and accrete to it by the subduction mechanism enlarging the continental mass. The next two snapshots stand for the early Proterozoic. For an age of 2070.2 Ma, Fig. 8b shows a central thermal plume streaming up to the asthenosphere. On the left a second plume developed that could not penetrate the 660-km discontinuity. Because of the high viscosity of the lower part of the lower mantle, the relative velocity of the two plumes is considerably less than the continent's velocity. One can hardly distinguish yet untouched parts of the mantle in the start position. The slight movements of the two plumes after 149.8 Ma have been recorded by Fig. 8c. Although the thermal bearings of the plumes mostly touch the lithosphere the ascended material often forms ptygmatic folds on a large scale in the upper mantle. Fig. 9 presents the development of the depleted mantle in the late Proterozoic and in the Phanerozoic. Substitutionally for a lot of other Rayleigh numbers, Rq, Fig. 9a and b shows that in the late Proterozoic the majority of the depleted regions assembled in the low-viscosity layer under the 660-km discontinuity. They sink very sluggishly whereas large new depleted areas develop in the upper mantle by chemical differentiation. For the ages 576.4 Ma, 246.4 Ma and for the geological present (0.1 Ma), Fig. 9c–e records the evolution of the bipartition of the mantle where the position of the plumes is rather stable. Nearly everywhere a depleted upper part of the mantle is situated proximately under the lithosphere. So, the uniformity of MORB can be explained. About half of the model mantle is depleted in the present. This result is

correspondent with geochemical findings. According to Taylor and McLennan (1995), 41.2% of the surface area of the real Earth is covered with continents, the average thickness of which is 39 km according to Christensen and Mooney (1995) or 41 km according to Abbott et al. (1997). The continental percentage of the whole model lithosphere is 36.3% in Fig. 9e. We investigated our model K2A for a large span of Rayleigh numbers. The main result is the evolution of the two principal mantle reservoirs and the CC. For the geological present we received a depleted upper part of the mantle, a lower part of the mantle rich in incompatible elements and a continent in the proper order of magnitude. This result proved to be very robust. For $Rq = 1.5 \times 10^6$, 2.0×10^6 and 4.0×10^6, Fig. 9eFig. 10a and b show that the depleted mantle is situated in the upper half. Its volume and that of the continent correspond with the observed values. However, the geophysical results like flow velocities, heat flow, continent velocity, temperature, viscosity, the function F, kinetic energy, etc. are very good only up to a Rayleigh number of $Rq = 2.4 \times 10^6$. Fig. 10c describes for $Rq = 7.0 \times 10^6$ and Fig. 10d shows for even $Rq = 2.0 \times 10^7$ that the geochemical subdivision is right in the prevailing trend. However, the depleted areas of the present diminish with growing Rq, that means they have a too small volume in comparison with the geochemical prediction but in all cases they are situated in the *upper* half of the mantle.

3.3. Some remarks on heat transport and the penetrability of the 660-km discontinuity

Christensen (1984) investigated the relation between the Nusselt number and two kinds of Rayleigh numbers for 2D *steady-state* convection in a square box with temperature-dependent viscosity. The convection of his model is driven by a given temperature contrast. The temperatures are fixed on top and bottom. So, the ratio of the highest viscosity to the lowest viscosity is fixed, too. Therefore and for other reasons we cannot expect complete comparability of our results with those of Christensen. The present model, K2A, is more complex. In particular, the viscosity ratio is not fixed but it is evolving during a run. Moreover, our *time-dependent* convection model is heated from within in a complex manner. Therefore, it is not possible to define some quantities in exactly the same kind. In order to compare it with one of Christensen's Rayleigh numbers, Ra_T, we introduce an auxiliary Rayleigh number, Ra_2,

$$Ra_2 = Ra_2(t) = \frac{\rho_0 \alpha g h^3}{\kappa \eta_{mean}} T_{mean} \qquad [D] \qquad (26)$$

where we also determine the mean viscosity, η_{mean}, as a function of the mean temperature, T_{mean}, but in a slightly altered way, namely by

$$\eta_{mean} = \eta_{01} \exp\left[\frac{E_0 + V_0 p_{dim,1/2}}{R T_{mean}(t)}\right] \qquad [D] \qquad (27)$$

where $T_{mean}(t)$ is the arithmetic mean of the dimensional temperature values at the gridpoints at a time t. The quantity $p_{dim,1/2}$ is the dimensional pressure in half a mantle depth according to PREM. In contrast to our scaling Rayleigh number, Rq, the auxiliary Rayleigh number, Ra_2, is a function of time. The Nusselt number is defined by

$$Nu = Nu(t) = \frac{q_{ob}(t)}{q_{ob,cond}(T_{mean}(t))} \qquad [D] \qquad (28)$$

where

$$q_{ob,cond} = \frac{8}{3} \frac{k}{h} T_{mean}(t) \qquad [D] \qquad (29)$$

(and $k = \kappa c_p \rho_0$) since we assumed heating from within. The other quantities of the last five formulae are given in Table 3. Similarly as Christensen found a rising Ra_T with a growing Nu for a constant viscosity ratio, we observe a rise of Ra_2 with ascending Nu. This relation is approximately fulfilled also

Fig. 9. The development of the geochemical reservoirs in the late Proterozoic and in the Phanerozoic for $Rq = 1.5 \times 10^6$. The snapshots represent the ages of 960.7, 808.7, 576.4, 246.4 and 0.1 Ma. The sequence of pictures shows a growing volume, depleted in incompatible elements, in the upper part of the mantle. Although the phase boundaries and the very high viscosity in the lower half of the lower mantle hinder the convection they do not prevent convection and mixing. Nevertheless, the interplay between fractionation and convection produces an upper half of the mantle which is depleted in radiogenic sources. The denotation of signs and hatchings is given in Section 3.2.

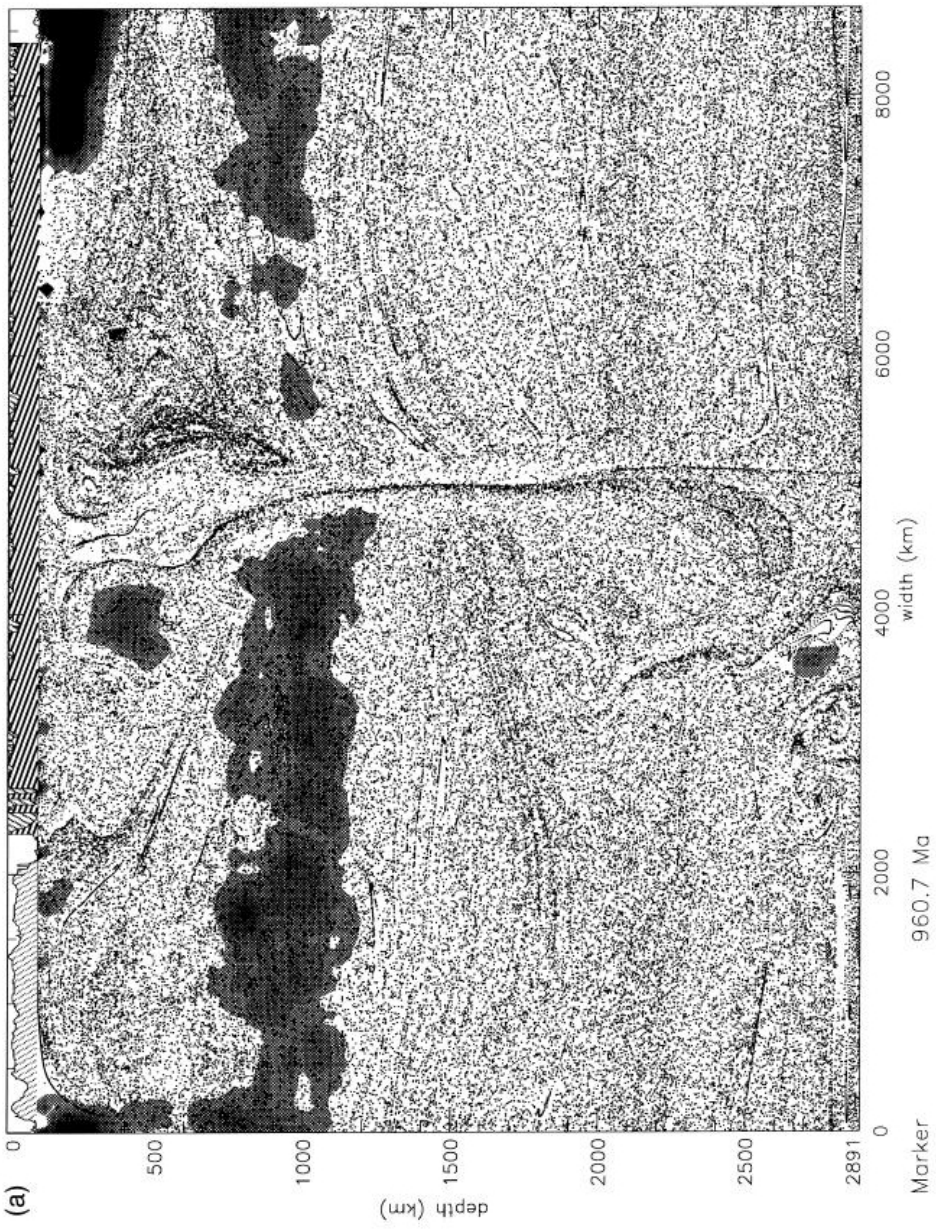
(a)
0
500
1000
1500
2000
2500
2891
depth (km)
0
2000
4000
6000
8000
width (km)
Marker
960.7 Ma

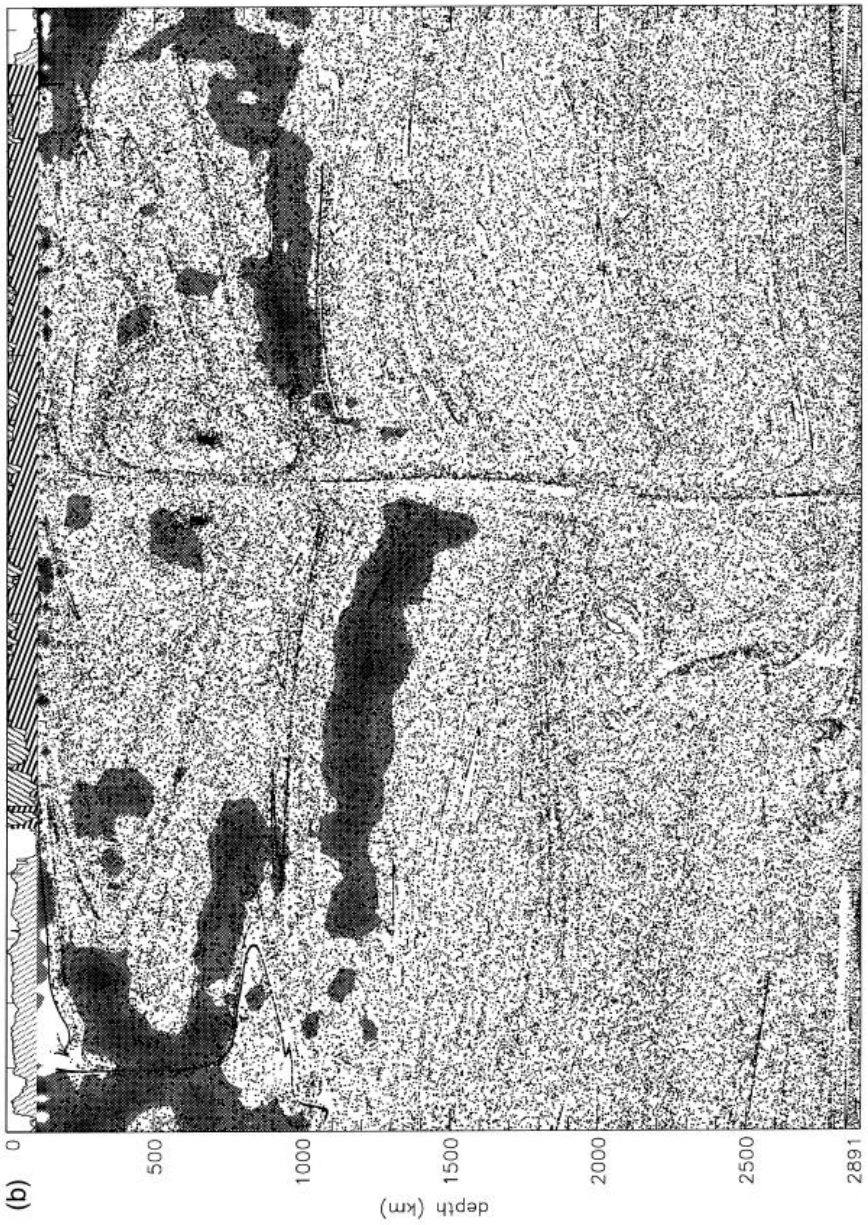

Fig. 9 (continued)

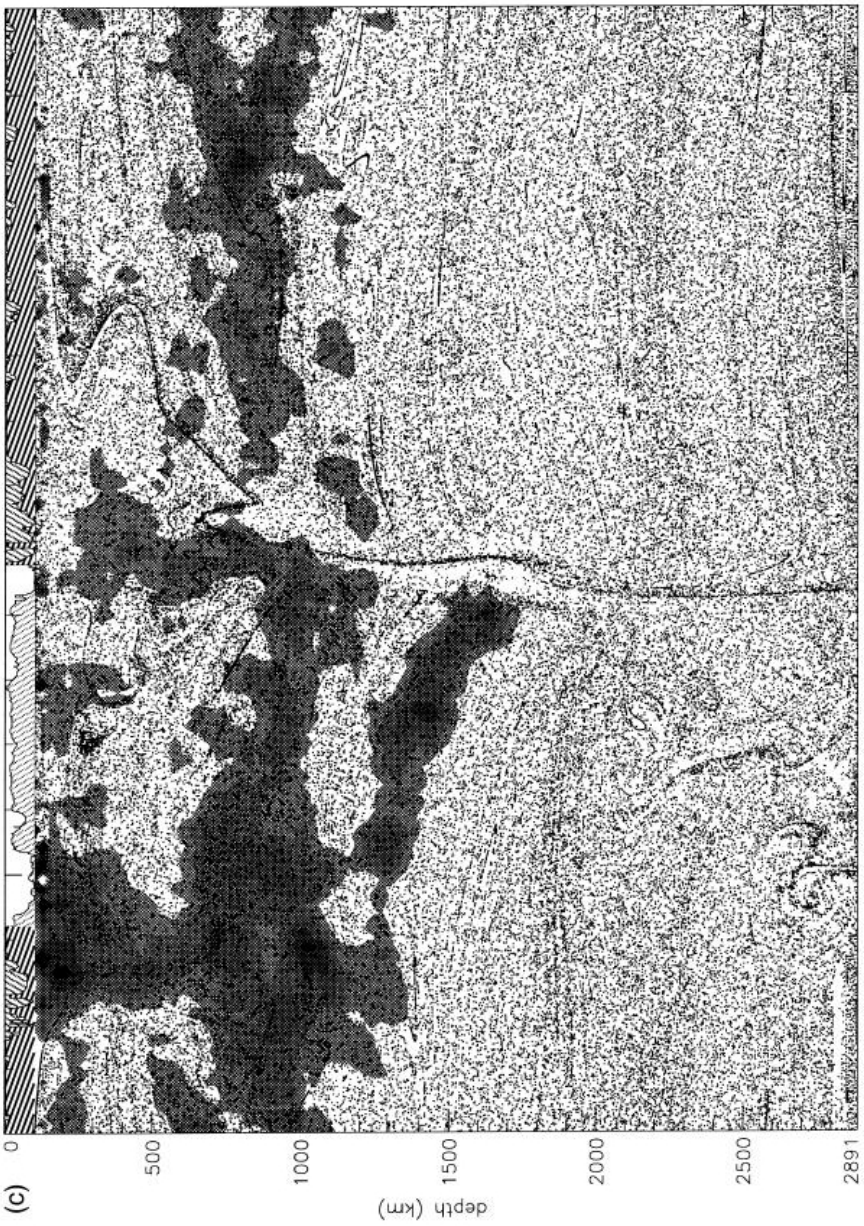

Fig. 9 (continued).

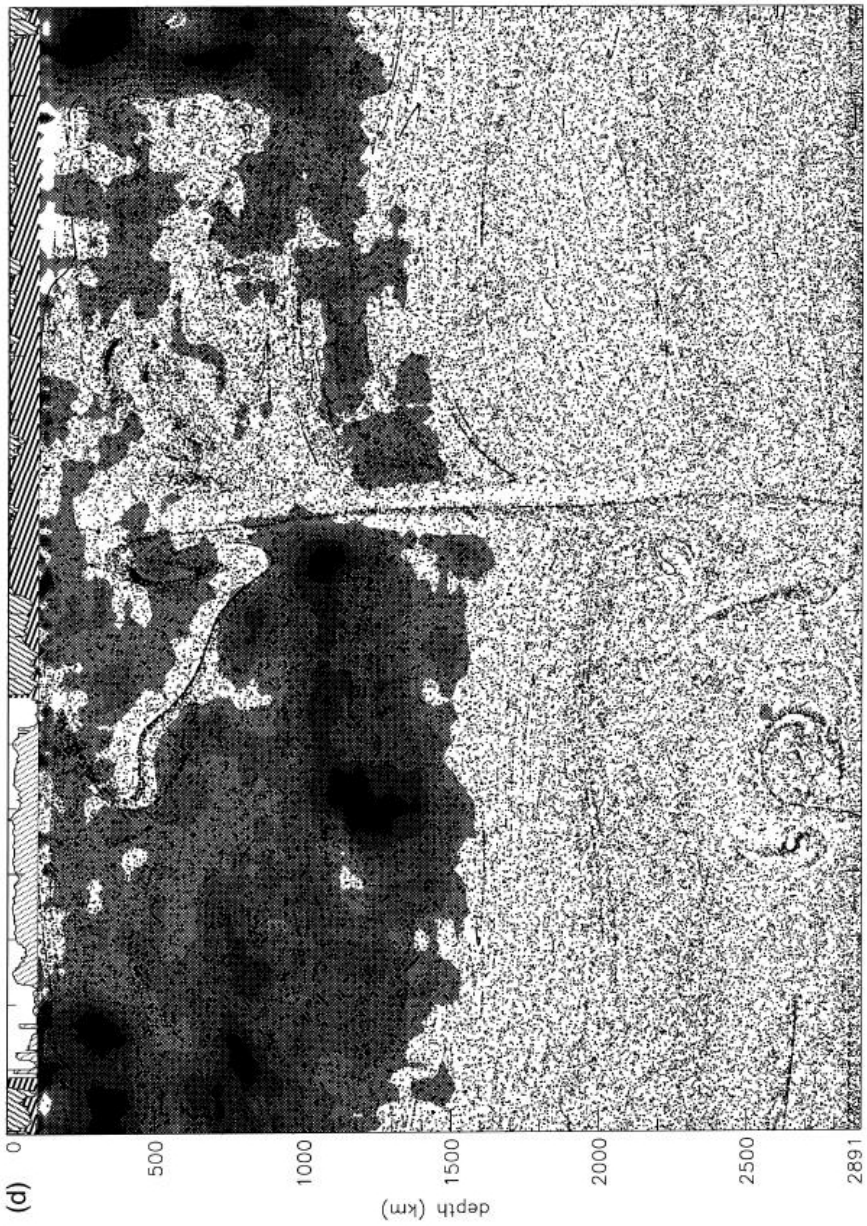

Fig. 9 (continued).

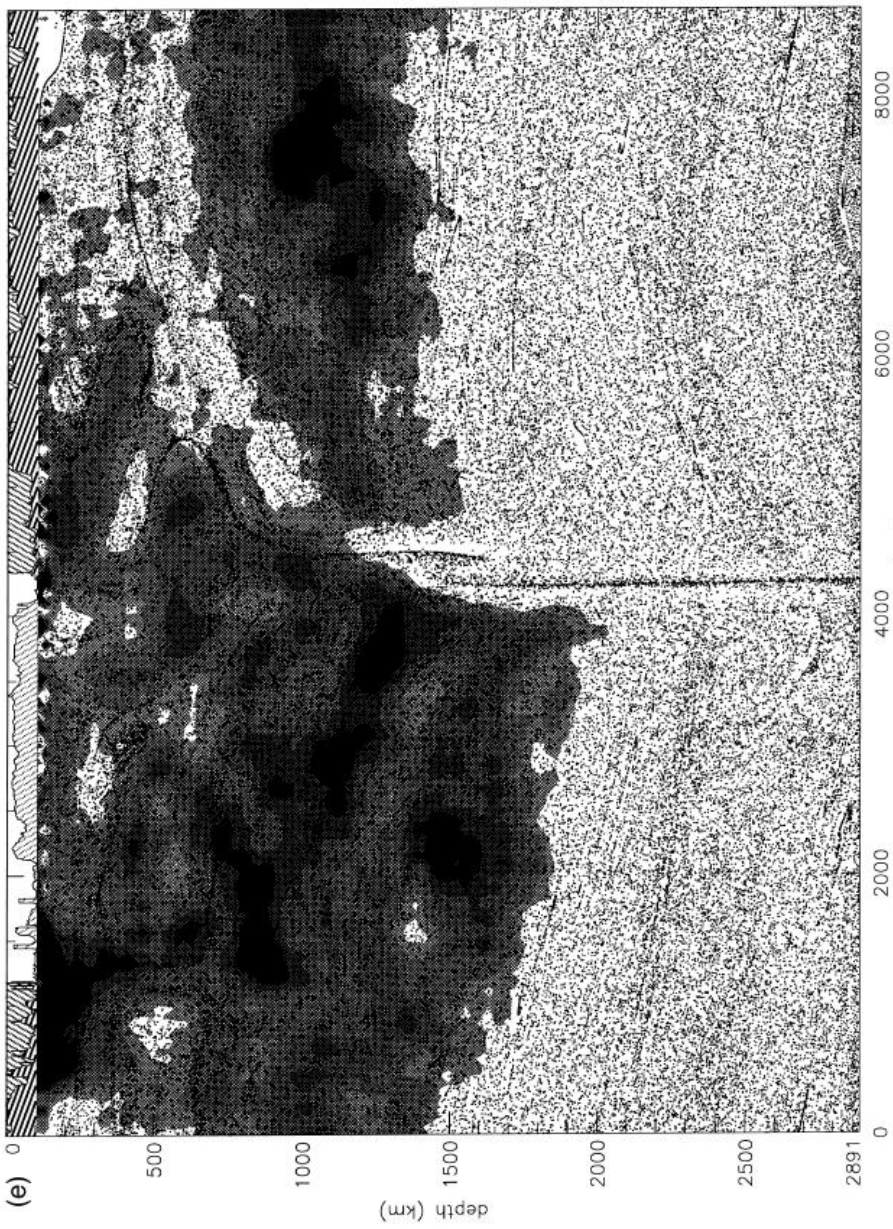

Fig. 9 (continued).

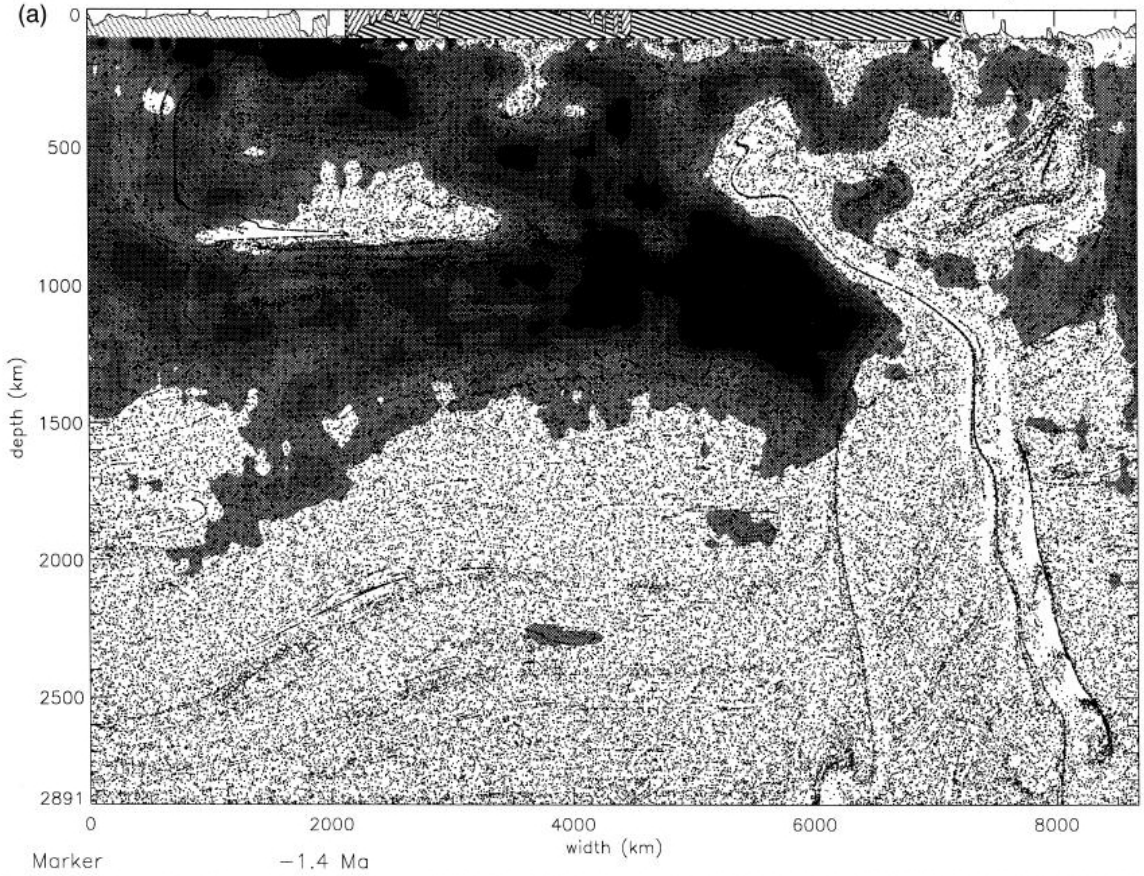

Fig. 10. The final stage of the evolution of the geochemical reservoirs for different Rayleigh numbers, Rq. (a) stands for Rq = 2.0×10^6, (b) for 4.0×10^5, (c) for 7.0×10^5 and (d) for 2.0×10^7. The definition of signs and hatchings is to be found in Section 3.2.

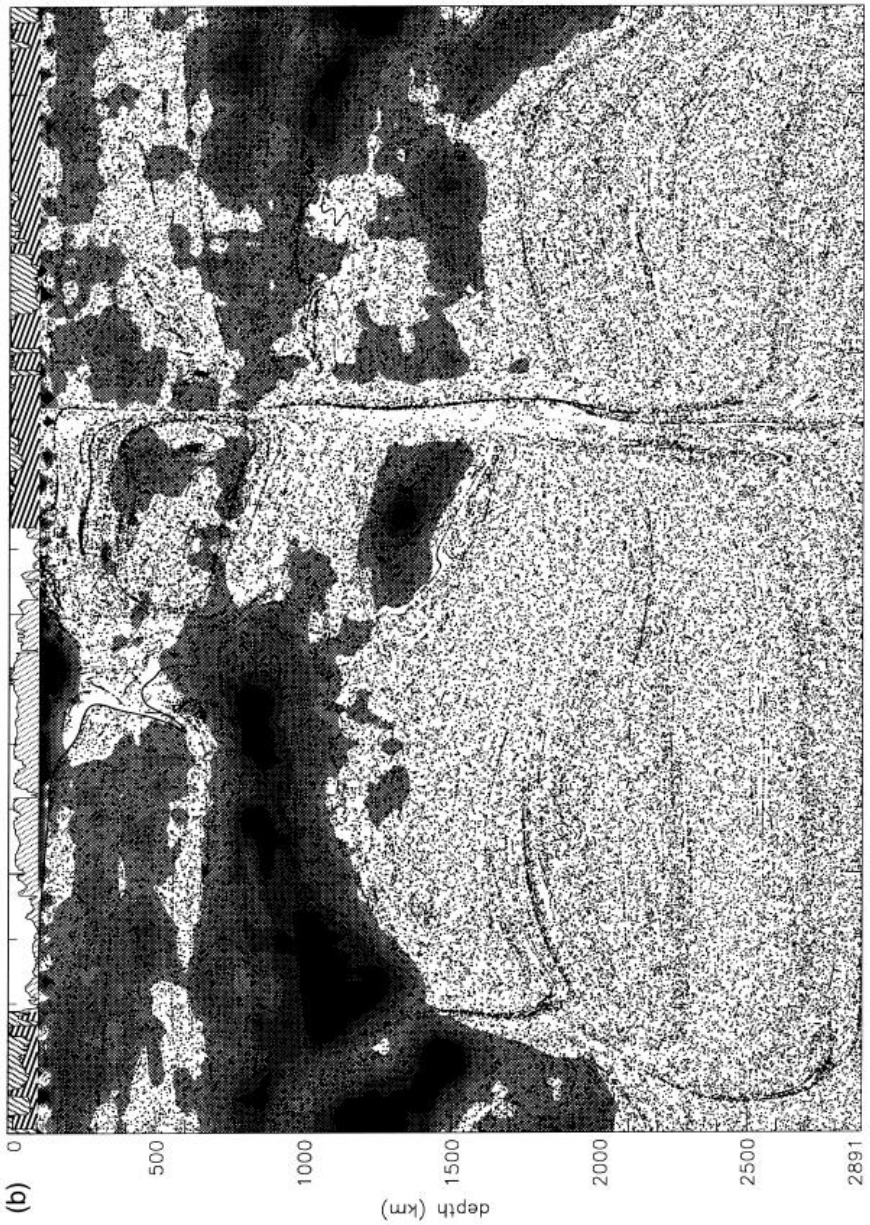

Fig. 10 (continued).

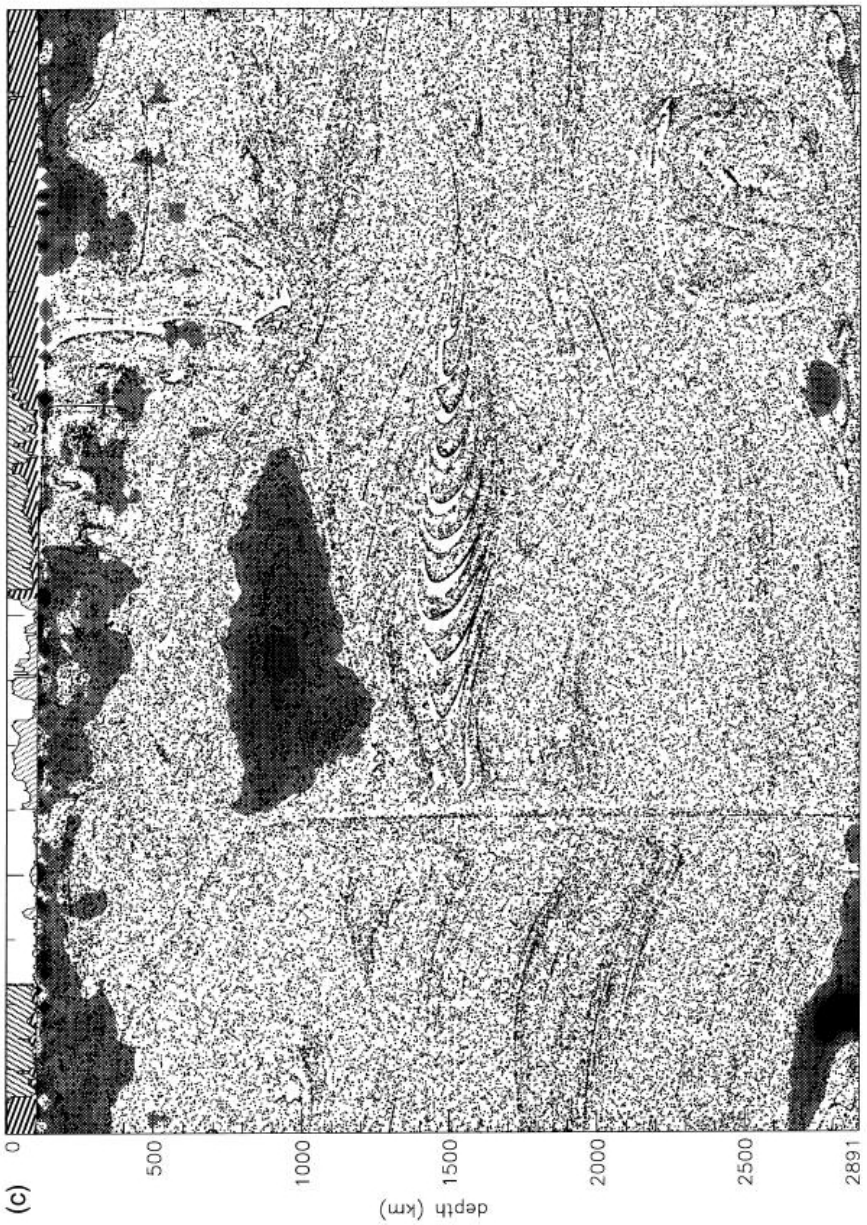

Fig. 10 (continued).

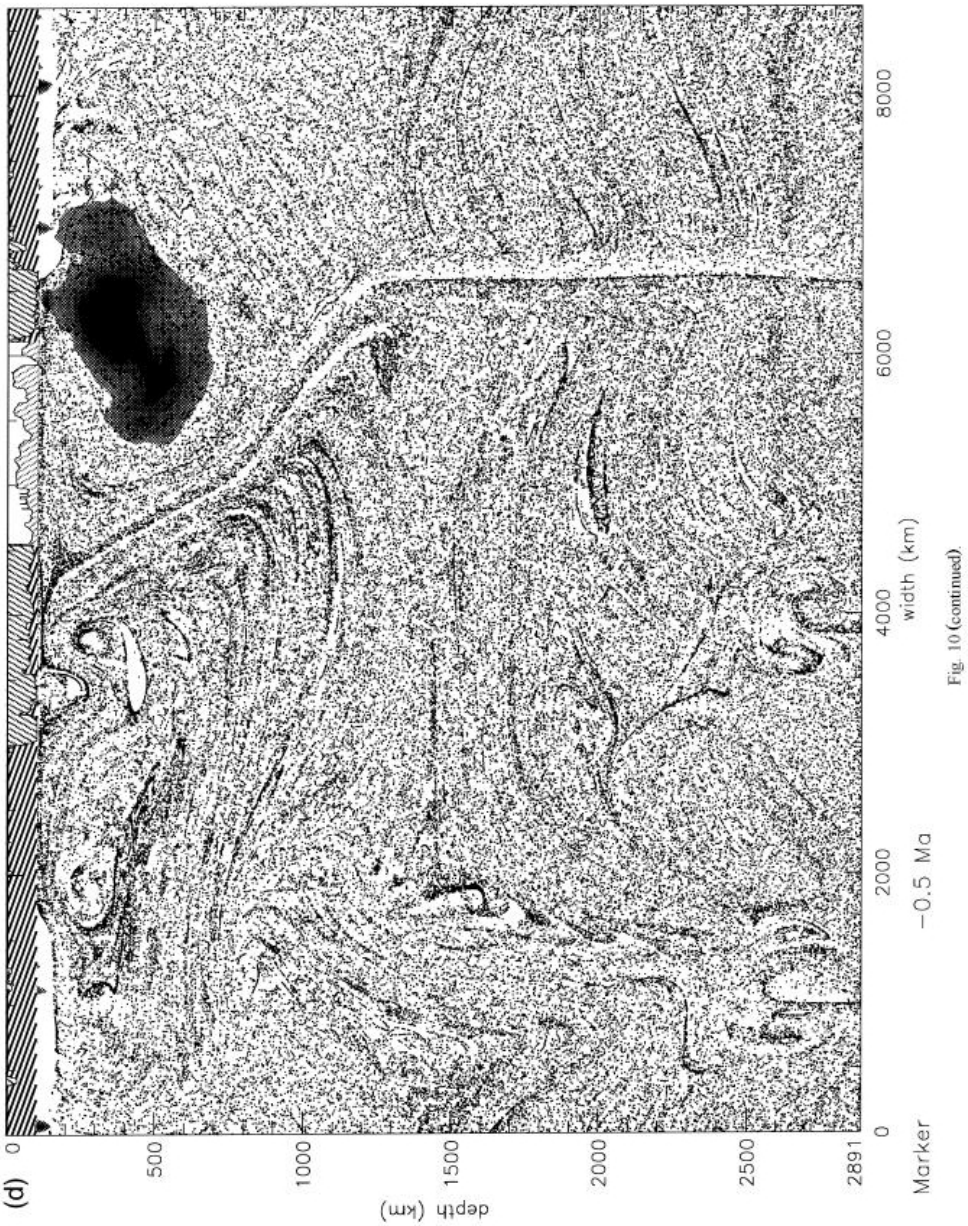

Fig. 10 (continued).

for a run with constant Rq although in this case the viscosity ratio is not exactly constant. An example is given in Table 4. It shows earth-like Nusselt numbers between 10 and 15. This result is very robust. It applies in this form for scaling Rayleigh numbers up to $Rq = 7 \times 10^6$.

Now we briefly debate the question whether two-layer convection or whole-mantle convection prevails in the mantle. We use some items of a catalogue of controversial questions discussed by Poirier (1991). *Proposition*: There are no earthquakes deeper than 670 km. The deep quakes have down-dip compression mechanisms. Therefore, the slabs cannot penetrate. *Answer*: Some slabs do not penetrate, other slabs break through into the lower mantle. In the pictures of our model we found both cases. The lack of earthquakes beneath 670 km is caused by the found second low-viscosity layer. But it is true that not only the 660-km phase boundary but also the transition zone with augmented viscosity (Spada et al., 1992) is an obstacle for the slab movement. Therefore down-dip compression mechanisms are produced by the slab penetrating the transition layer. The slabs *can* move into the lower mantle but the transition layer and the 660-km phase boundary hinder the slab in its break through. Two further *propositions*: The 660-km discontinuity is also a compositional boundary (Liu, 1979; Anderson, 1989). The upper and lower mantle are two different geochemical reservoirs (Allègre, 1982). *Answer*: Concerning the gross chemical composition there are good arguments that the mantle is in some degree homogeneous (O'Neill and Palme, 1998). Referring to the abundances of incompatible elements the mantle is divided in two physically distinct principal reservoirs and some minor reservoirs (Hofmann, 1988; Hart and Zindler, 1989). In the present paper we have shown that, in spite of the partial penetrability of the 660-km discontinuity and in spite of the convective mixing, for acceptable Rayleigh numbers the model mantle arrives at a bipartition in a depleted upper half and a lower half that is richer in incompatible elements. The boundary of the two halves is, of course, not at the 660-km discontinuity. A fourth *proposition*: The 660-km boundary is a sharp seismic reflector and the corresponding phase transition occurs over a wide depth span. Therefore it must also be a compositional boundary in the main constituents. *Answer*: The spinel–perovskite plus magnesiowüstite transition is sharp. A chemical difference is not necessarily required (Ito and Takahashi, 1989). Our results show that there is neither strictly layered convection nor whole-mantle convection in the original sense of the word but a kind of leaky two-layer convection with chemical fractionation.

Table 4
The evolution of the auxiliary Rayleigh number, Ra_2, and the Nusselt number, Nu, for $Rq = 1.5 \times 10^6$

Age (Ma)	Ra_2	Nu
3049.8042	40253486	12.424821
2545.1768	62827719	13.123430
2049.9083	66020994	13.279340
1549.7533	22640413	12.586531
1049.8467	42958912	14.721472
548.8635	15904268	11.193636
0.0927	10478461	10.923276

4. Conclusions

Starting from a primordial mantle with two phase transitions in 410 and 660 km of depth, we model simultaneously the origin and evolution of the CC by chemical segregation *and* the mantle flow by two-dimensional and finite-difference Oberbeck–Boussinesq thermal convection. Oceanic plateaus develop from enriched melts by chemical differentiation. The latter process leaves behind mantle areas depleted of radiogenic isotopes. At first, some terranes unite occasionally, then the continent grows systematically by accretion of terranes in an accretional wedge. The irregular distribution of the depleted parts of the early upper mantle generates a first feedback mechanism. A second feedback mechanism is caused by the lateral movability of the continents. Both of them and the time dependence of the radiogenic decay generate a time-dependent model convection. At first, we investigate the lateral velocity of the continent, the juvenile continental volume growth rate, the average surface heat flow, the convective vigor of the upper and the lower mantles and the mean temperature of the mantle as a function of time as well as the distribution of the surface heat flow on

continent and ocean. Of course, no model can account for all the complexities occurring in the Earth. Our model yields a realistic course of the horizontally averaged surface heat flow and of the lateral continental velocity as a function of time. The time dependence of the growth of juvenile continental mass has a resemblance to the distribution of supercontinental cycles (cf. Worsley et al., 1986). Of course, this is no deterministic proof of such a connection. But there is a probability to explain orogenetic activity epochs in this way. At the start of the Phanerozoic, about 50% of the model continental mass already exist. This corresponds to the observation. We received a realistic viscosity distribution in the mantle (Fig. 5). The upper area, corresponding to the MORB source, has a low viscosity and high absolute values of the creeping velocity. Both are in the right order of magnitude. So it is understandable that MORB is homogenized and mixed thoroughly. Tubes of low viscosity cross the highly viscous area of the lower half of the mantle. The lateral velocity of the plumes is considerably lower than the lithospheric plate velocity. In this way, the model plumes form a reference frame for the movements of the lithospheric plates. However, the main result is that the depleted mantle forms the upper half of the mantle and that it is mixed only to a minor degree with the rest of mantle which is rich in incompatible elements, yet.

We presuppose only a 20 mW m^{-2} heat flow at the CMB. The mantle is mainly heated from within by the dynamically fluctuating inhomogeneous distribution of ^{238}U, ^{235}U, ^{232}Th and ^{40}K. The temperature dependence of the viscosity is an essential feature of the model. So the viscosity depends upon both the vertical component of the location vector and also on the horizontal one and the time. On the other hand, we compute snapshots of the temperature, viscosity and stream-function distribution in the mantle. The solutions show *a depleted upper half of*

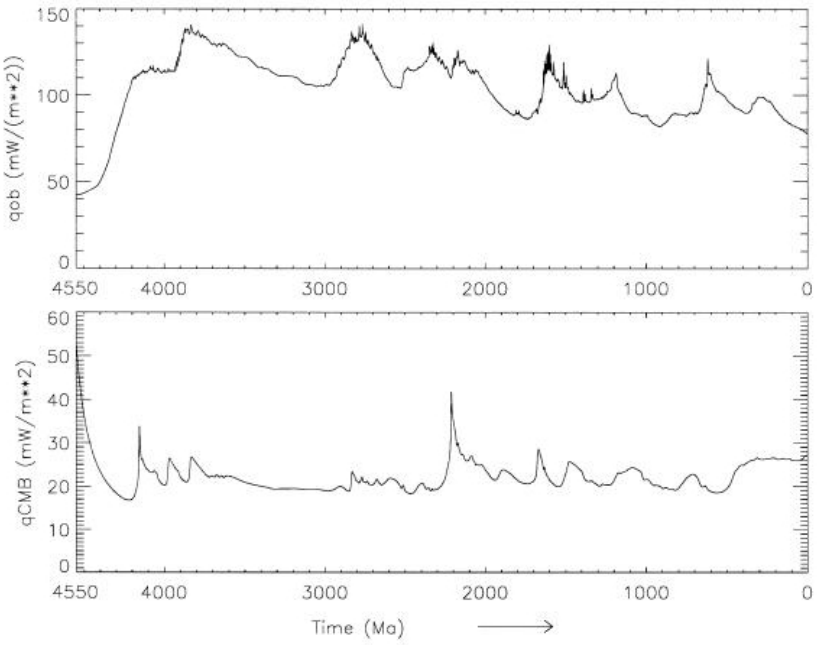

Fig. 11. In the upper panel, the evolution of the horizontally averaged heat flow q_{ob} at the Earth's surface is depicted where we exceptionally assumed that the temperature at the core–mantle boundary is constant: $T_{CMB} = 4610$ K. The lower panel gives the laterally averaged heat flow q_{CMB} at the core–mantle boundary for the same run. Rq $= 1.5 \times 10^6$.

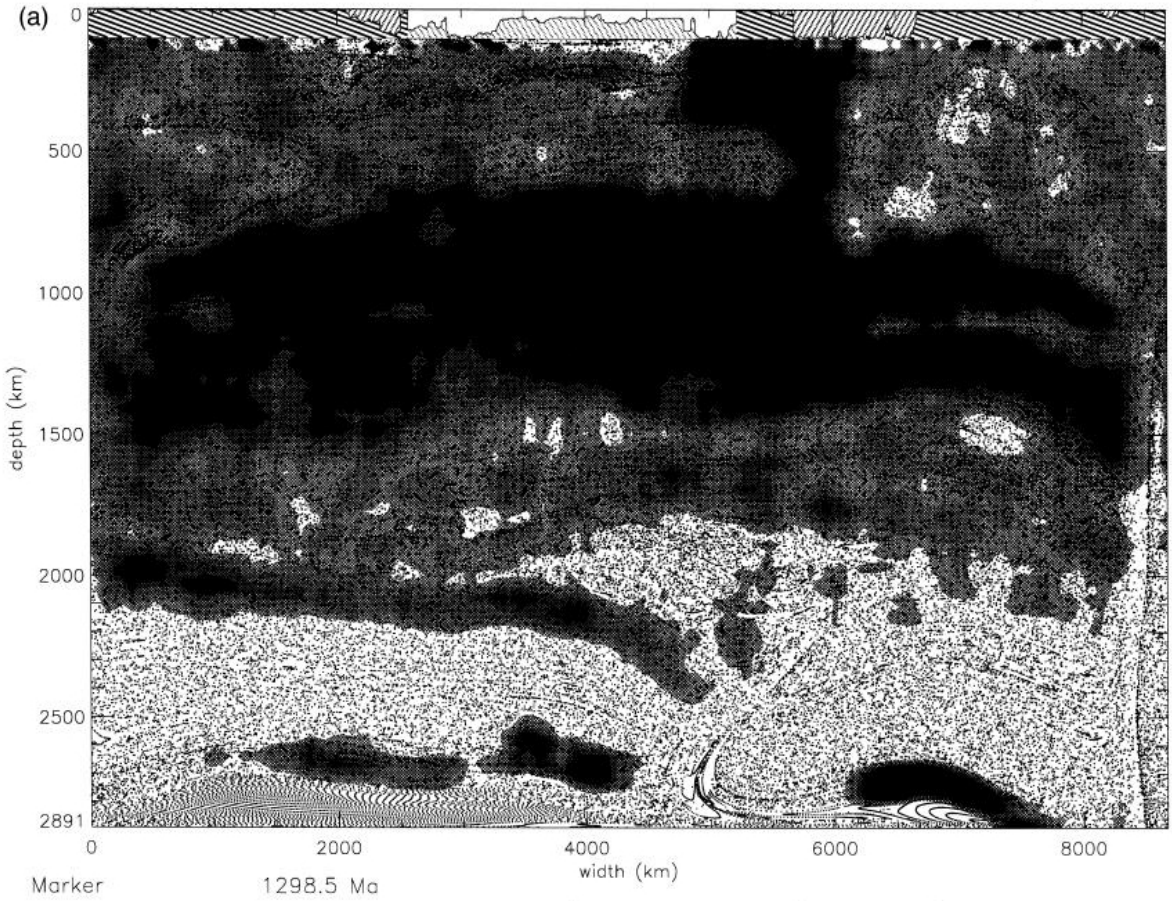

Fig. 12. The evolutionary state of the geochemical reservoirs in the late Proterozoic (a) and in the geological present (b) for $Rq = 1.5 \times 10^6$ and $T_{CMB} = 4610$ K. The definition of signs and hatchings is to be found in Section 3.2.

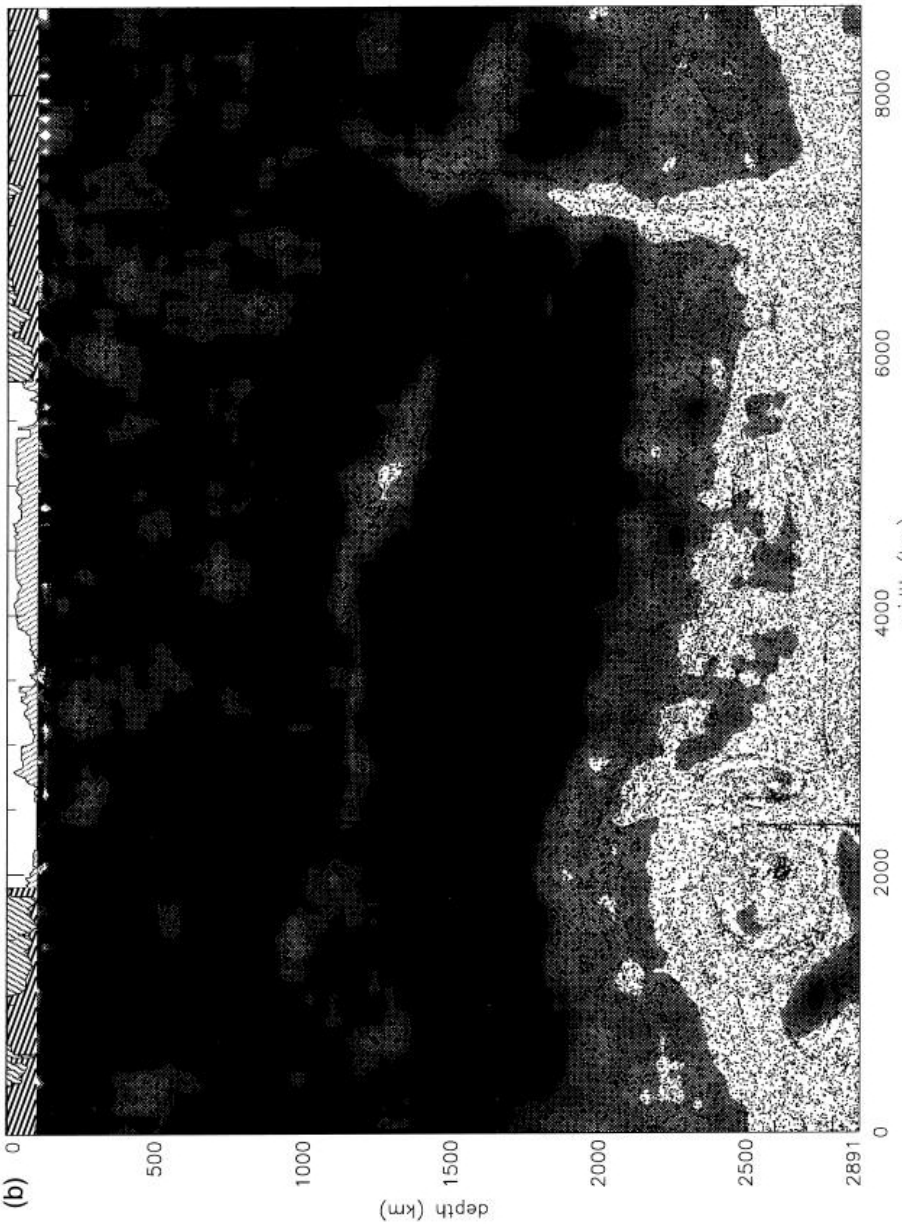

Fig. 12 (continued)

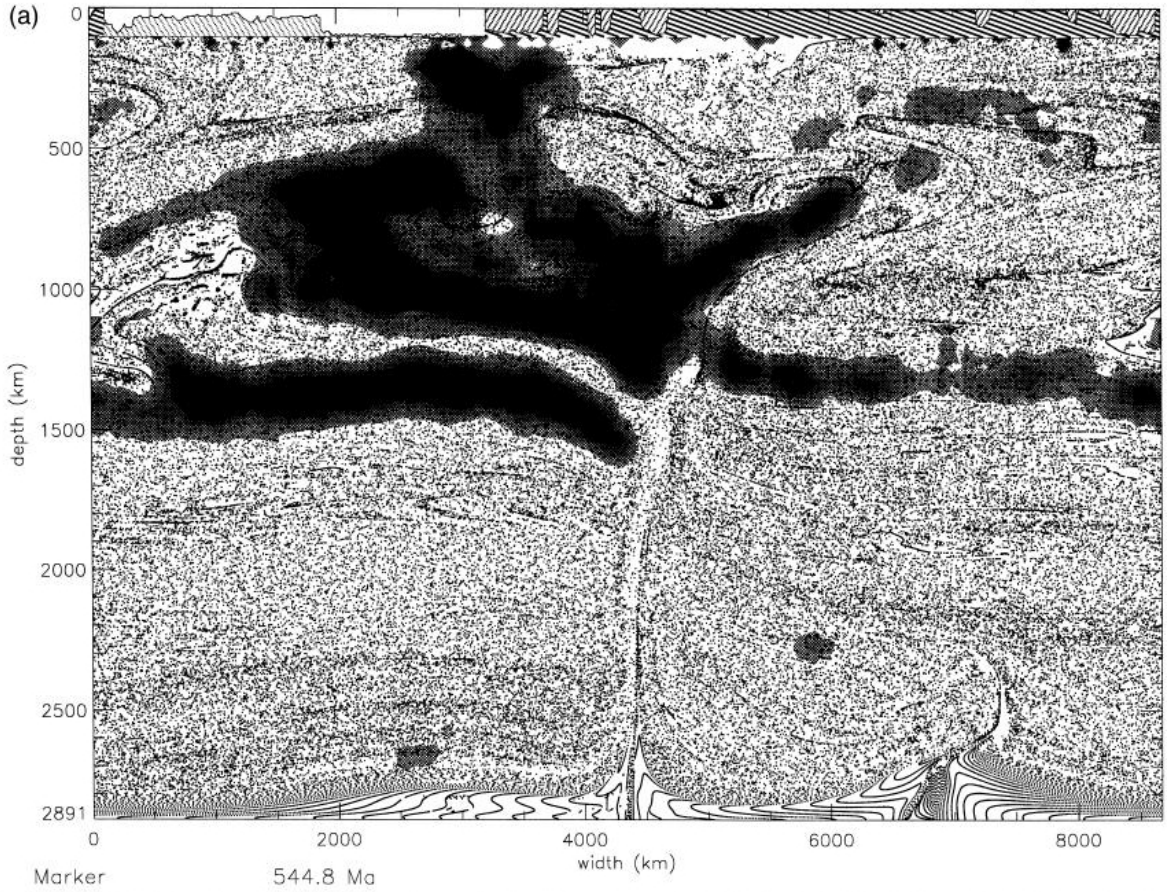

Fig. 13. Two snapshots of the geochemical reservoirs in the early Paleozoic (a) and in the geological present (b) for $Rq = 1.5 \times 10^6$ and $T_{CMB} = 3750$ K. The denotation of signs and hatchings is given in Section 3.2.

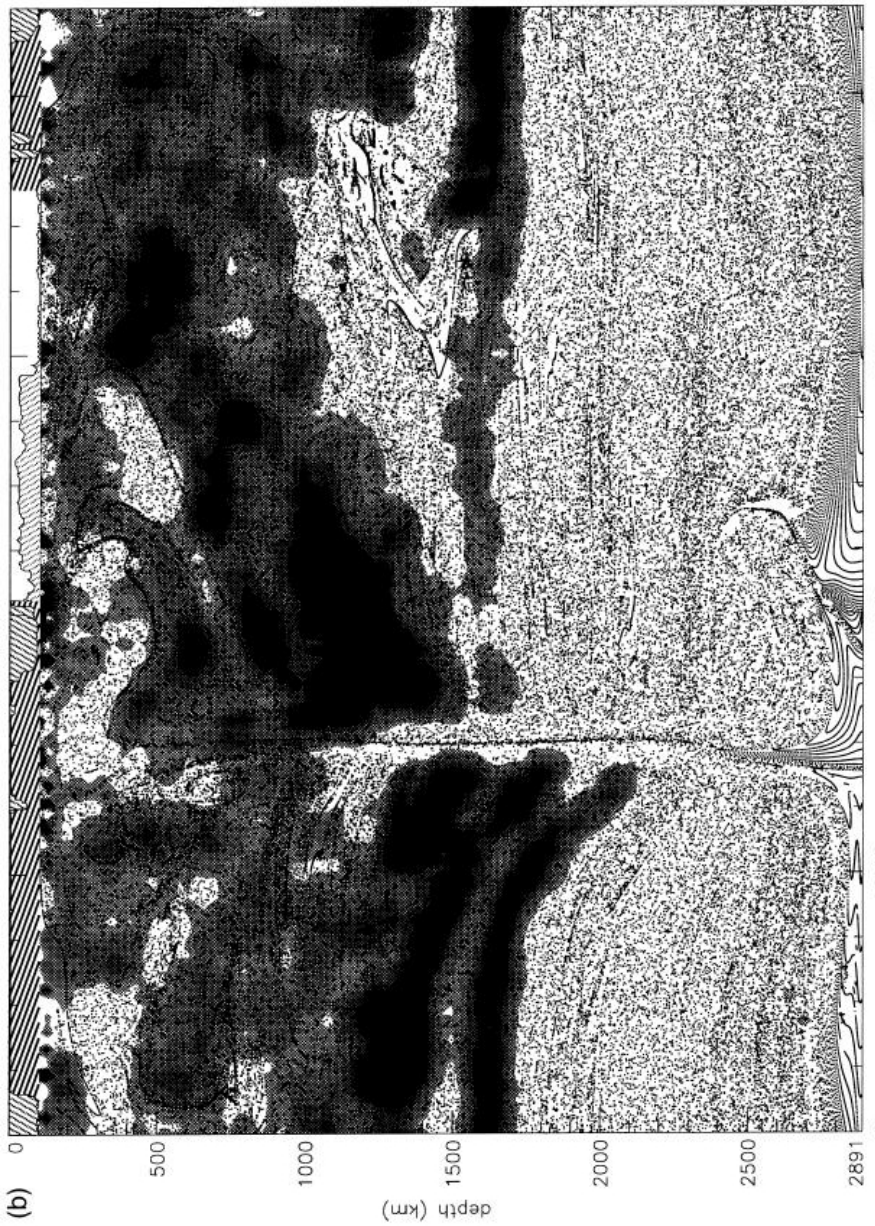

Fig. 13 (continued).

the present mantle and acceptable values for the continental growth and for the distribution of temperature, viscosity and of the velocity of creep in the mantle.

It is remarkable that the excellent correspondence of the *geophysical* results of our model with observational results is confined to a surrounding of $Rq = 1.5 \times 10^6$ and to the interval of $2.0 \times 10^6 \leq Rq \leq 2.4 \times 10^6$ whereas the *geochemical* bipartition of the present mantle in an upper depleted half and in a lower half, rich in incompatible elements, and the right partition of the lithosphere in a lithosphere with oceanic MORB crust, oceanic plateaus and continental plate apply for about $1.5 \times 10^6 \leq Rq \leq 4.0 \times 10^6$, in outlines even for higher Rq values yet.

Acknowledgements

We thank Harro Schmeling for kindly providing his code for the calculation of 2D thermal convection. We used it as a starting variant for the development of our K1 code which is the forerunner of the present K2A code with chemical differentiation. Furthermore, we gratefully acknowledge the helpful discussions and comments of the reviewers.

Appendix A

Some items are to be explained here in detail. First, the thermal boundary condition at the core–mantle boundary (CMB) is discussed in detail. At the Earth's surface, the temperature is kept more or less constant since more than 3.8×10^9 years. This mechanism depends on the global carbon cycle and on the existence of life. Irrespective of whether this explanation is right, the temperature stability at the surface can be considered as an observational fact because of the long existence of fluviatile and organic sediments. As far as we know, there is no such thermostat at the CMB. One of our referees remarked that we know that the mean temperature of the Earth decreases by about 100 K per billion years. This is right. Our model K2A shows that the mean temperature of the mantle fell by 400 K in the last 3700 Ma. This is a good coincidence with observation. Therefore it is also very probable that the laterally averaged CMB temperature dropped somewhat during the evolution of the Earth. So, the CMB temperature should *not* be a constant with respect to *time*. This is caused by the fact that the mantle is essentially heated from within. On the other hand, we can expect that the CMB temperature is virtually *laterally* constant because of the very low viscosity of the outer core: 1 to 100 Pa s or even lower. Lister and Buffett (1995) deduced a new expression for the dynamo efficiency in terms of Carnot-style redistribution of heat and mass in the core. The present-day heat loss across the CMB is estimated to be caused by an 80% contribution of compositional outer-core convection and a 20% contribution of thermal outer-core convection. Lister and Buffett arrive at a CMB heat flux of 2.7×10^{12} W. We conclude from it a CMB heat flux density of 17.74 mW m^{-2}. Stacey (1992) investigated the dynamo from the thermodynamic point of view and computed 3.7×10^{12} W for the conducted heat down the adiabatic gradient. He emphasized that it is not necessary for all of this heat to be conducted into the mantle because some may be carried down again by the compositional outer core convection. In this way, we receive an *upper bound* of the heat flux density of 24.31 mW m^{-2}. In his Section 6.7.5 entitled Constancy of the Core-to-Mantle Heat Flux, Stacey (1992) drew the attention to the fact that the inner-core growth must be possible and *simultaneously* the dynamo mechanism must be fed for a sufficiently long time span. There must be left enough power for the dynamo. Loper (1984) revealed by an investigation into the D''-plume mechanism that the CMB heat flow must have been remarkably steady in the Earth's history. Stacey (1992) estimated a CMB heat flux of 3.0×10^{12} W. Independently, Sleep (1990) concluded a CMB heat flux of 3.0×10^{12} W. His investigation is based on the heat transport of mantle plumes. We convert this value in a CMB heat flux density of 19.7 mW m^{-2}. Therefore we are entitled to assume a constant core-to-mantle heat flow density of 20 mW m^{-2} for our model K2A. For the mentioned reasons, a CMB temperature constant with respect to time would be a less good approach for calculations of the long time span of the Earth's evolution.

However, in order to dispel doubts about the robustness of our model we want to introduce an

auxiliary variant of it exclusively in this Appendix. In this variant, we renounce the constancy of CMB heat flux density and introduce a CMB temperature that is constant laterally *and* with respect to time. In order to have a good comparability with Figs. 3–9e (with $q_{CMB} = 20$ mW m^{-2}), we compare only runs with the same parameters and details of the model except the thermal boundary condition at CMB. According to Boehler (1997), the *minimum* temperature at CMB is 4000 K.

In the *first* example, we use therefore the temporally *and* laterally averaged CMB temperature value of the mentioned run of comparison. So we assume here $T_{CMB} = 4610$ K. In spite of it we receive moderate temperatures only a few degrees higher than 2000 K for two thirds of the mantle. Only the upper parts have lower temperatures, whereas a steep gradient can be observed near the CMB. The upper panel of Fig. 11 shows the evolution of the laterally averaged surface heat flow as a function of time. The order of magnitude of this surface heat flow, the since an age of 3800 Ma weakly monotonously falling course of the smoothed part of the curve and the frequency content of the superposed fluctuations are very similar to Fig. 3. The lower panel of Fig. 11 represents the laterally averaged CMB heat flow. As things now stand, its course as a function of time has, naturally, also variations. Its average value in a sliding window is temporally rather stable and is only slightly higher than 20 mW m^{-2}. Fig. 12a depicts the result of the chemical evolution for an age of 1298.5 Ma, Fig. 12b represents the chemistry for the geological present. Although the growth of the depleted mantle and of the continent is a little too fast, in both pictures there is, first, a distinctly separated depleted mantle in spite of partial blend and, secondly, a position of the depleted mantle in the upper parts of the mantle.

The *second* example uses the estimate of Stacey (1992) for the CMB temperature of $T_{CMB} = 3750$ K. We have a bipartition of the mantle into an upper depleted part and a lower part rich in incompatible elements. Fig. 13a shows this result for an age of 544.8 Ma, Fig. 13b for the present day, respectively. The growing continent and the oceanic plateaus are depicted in the upper parts of the two figures. The 41.2% surface area of the real Earth is covered with continent. This is between the computed 45.0% of Fig. 12b and the 36.5% of Fig. 13b. Also the shares of the depleted mantle are above and below the expected value, respectively. For the less realistic case of a constant CMB temperature, this value should be between 4610 and 3750 K, probably closer to 4610 K. It can be summed up to the effect that the change to constant T_{CMB} altered the bipartition mechanism only slightly.

Appendix B

Here, non-dimensional variables are introduced. They are designated by primes.

Horizontal component of the location vector	$x = hx'$
Vertical component of the location vector	$z = hz'$
Density	$\rho = \rho_0 \rho'$
Time	$t = (h^2/\kappa)t'$
Stream function	$\psi = \kappa\psi'$
Temperature	$T = [(Q_0 h + q_{CMB})h/k]T'$
Horizontal component of the velocity	$u = (\kappa/h)u'$
Vertical component of of the velocity	$w = (\kappa/h)w'$
Pressure	$p = (\kappa\eta_0/h^2)p' - \rho_0 ghz'$
Viscosity	$\eta = \eta_0\eta'$
Viscosity coefficient in Eq. (18)	$\eta_{0\lambda} = \eta_0\eta'_{0\lambda}$
Viscosity in a part of the mantle labeled with λ	$\eta_\lambda = \eta_0\eta'_\lambda$
Specific heat production	$H = H_0 H'$
Specific isotopic heat prodution $4.55 \times 1o^9$ years ago	$H_{0\nu} = H_0 H'_{0\nu}$

Magnitude of the heat flow	$q = (Q_0 h + q_{CMB}) q'$
Clapeyron slope of the kth phase transition	$\gamma_k = [\rho_0 g k / (Q_0 h + q_{CMB})] \gamma_k'$

References

Abbott, D.A., Drury, R., Mooney, W.D., 1997. Continents as lithological icebergs: the importance of buoyant lithospheric roots. Earth Planet. Sci. Lett. 149, 15–27.

Allègre, C.J., 1982. Chemical geodynamics. Tectonophysics 81, 109–132.

Allègre, C.J., Brevart, O., Dupré, B., Minster, J.F., 1980. Isotopic and chemical effects produced in a continuously differentiating convecting Earth mantle. Philos. Trans. R. Soc. London, Ser. A 297, 447–477.

Anderson, D.L., 1989. Composition of the Earth. Science 243, 367–370.

Armstrong, R.L., 1991. The persistent myth of crustal growth. Aust. J. Earth Sci. 38, 613–630.

Baumgardner, J.R., 1985. Three dimensional treatment of convective flow in the Earth's mantle. J. Stat. Phys. 39 (5–6), 501–511.

Baumgardner, J.R., 1988. Application of supercomputers to 3D mantle convection. In: Runcorn, S.K. (Ed.), The Physics of the Planets. Wiley, New York, pp. 199–231.

Boehler, R., 1996. Melting temperature of the Earth's mantle and core: Earth's thermal structure. Annu. Rev. Earth Planet. Sci. 24, 15–40.

Boehler, R., 1997. The temperature in the Earth's core. In: Crossley, D.J. (Ed.), Earth's Deep Interior. Gordon and Breach Sci. Publ., Amsterdam, pp. 51–63.

Bunge, H.-P., Richards, M.A., Baumgardner, J.R., 1997. A sensitivity study of three-dimensional spherical mantle convection at 10^8 Rayleigh number: effects of depth-dependent viscosity, heating mode, and an endothermic phase change. J. Geophys. Res. 102, 11991–12007.

Christensen, U.R., 1984. Heat transport by variable viscosity convection and implications for the Earth's thermal evolution. Phys. Earth Planet. Int. 35, 264–282.

Christensen, U.R., 1985. Thermal evolution models for the Earth. J. Geophys. Res. 90, 2995–3007.

Christensen, N.I., Mooney, W.D., 1995. Seismic velocity structure and composition of the continental crust: a global view. J. Geophys. Res. 100, 9761–9788.

Christensen, U.R., Yuen, D.A., 1984. The interaction of a subducting lithospheric slab with a chemical or phase boundary. J. Geophys. Res. 89, 4389–4402.

Christensen, U.R., Yuen, D.A., 1985. Layered convection induced by phase transitions. J. Geophys. Res. 90, 10291–10300.

Delano, J.W., Stone, K., 1985. Siderophile elements in the Earth's upper mantle: secular variations and possible causes for their overabundance. Lunar Planet. Sci. 16, 181–182.

Dupeyrat, L., Sotin, C., Parmentier, M., 1995. Thermal and chemical convection in planetary mantles. J. Geophys. Res. 100, 497–520.

Dupré, B., Allègre, C.J., 1983. Pb–Sr isotope variation in Indian Ocean basalts and mixing phenomena. Nature 303, 142–146.

Dziewonski, A.M., Anderson, D.L., 1981. Preliminary reference Earth model. Phys. Earth Planet. Int. 25, 297–356.

Fukao, Y., Obayashi, M., Inoue, H., Nenbai, M., 1992. Subducted slabs stagnant in the mantle transition zone. J. Geophys. Res. 97, 4809–4822.

Gottschaldt, K.-D., 1997. Periodische Randbedingungen bei der zweidimensionalen numerischen Modellierung von Konvektion im Erdmantel. Diplomarbeit, Friedrich-Schiller-Universität Jena, Germany.

Hart, S.R., 1984. A large-scale isotope anomaly in the Southern Hemisphere mantle. Nature 309, 753–757.

Hart, S., Zindler, A., 1989. Constraints on the nature and development of chemical heterogeneities in the mantle. In: Peltier, W.R. (Ed.), Mantle Convection. Gordon and Breach Science Publishers, New York, pp. 261–387.

Heinz, D.L., Jeanloz, R., 1987. Measurement of the melting curve of $Mg_{0.9}Fe_{0.1}SiO_3$ at lower mantle conditions and its geophysical implications. J. Geophys. Res. 92, 11437–11444.

Hofmann, A.W., 1988. Chemical differentiation of the Earth: the relationship between mantle, continental crust, and oceanic crust. Earth Planet. Sci. Lett. 90, 297–314.

Honda, S., Balachandar, S., Yuen, D.A., Reuteler, D., 1993. Three-dimensional mantle dynamics with an endothermic phase transition. Geophys. Res. Lett. 20, 221–224.

Ito, E., Takahashi, E., 1987. Melting of peridotite at uppermost lower-mantle conditions. Nature 328, 514–517.

Ito, E., Takahashi, E., 1989. Post-spinel transformations in the system Mg_2SiO_4–Fe_2SiO_4 and some geophysical implications. J. Geophys. Res. 94, 10637–10646.

Jacobsen, S.B., Harper, C.L., Jr., 1996. Accretion and early differentiation history of the Earth based on extinct radionuclides. In: Basu, A., Hart, S. (Eds.), Earth Processes: Reading the Isotopic Code. Geophys. Monogr. Am. Geophys. Union 95, pp. 47–74.

Jacobsen, S.B., Wasserburg, G.J., 1979. The mean age of mantle and crustal reservoirs. J. Geophys. Res. 84, 7411–7427.

Jochum, K.P., Hofmann, A.W., Seuferth, H.M., 1993. Tin in mantle-derived rocks: constraints on Earth evolution. Geochim. Cosmochim. Acta 57, 3585–3595.

Kameyama, M., Fujimoto, H., Ogawa, M., 1996. A thermo-chemical regime in the upper mantle in the early Earth inferred from a numerical model of magma-migration in a convecting upper mantle. Phys. Earth Planet. Int. 94, 187–215.

Kido, M., Čadek, O., 1997. Inferences of viscosity from the oceanic geoid: indication of a low viscosity zone below the 660-km discontinuity. Earth Planet. Sci. Lett. 151, 125–137.

King, S.D., 1995. Radial models of mantle viscosity: results from a genetic algorithm. Geophys. J. Int. 122, 725–734.

Knittle, E., Jeanloz, R., 1989. Melting curve of (Mg, Fe) SiO_3 perovskite to 96 GPa: evidence for a structural transition in lower mantle melts. Geophys. Res. Lett. 16, 421–424.

Kramers, J.D., Tolstikhin, I.N., 1997. Two terrestrial lead isotope

paradoxes, forward transport modelling, core formation and the history of the continental crust. Chem. Geol. 139, 75–110.
Lister, J.R., Buffett, B.A., 1995. The strength and efficiency of thermal and compositional convection in the geodynamo. Phys. Earth Planet. Int. 91, 17–30.
Liu, L.G., 1979. On the 650 km seismic discontinuity. Earth Planet. Sci. Lett. 42, 202–208.
Loper, D.E., 1984. The dynamical structure of D'' and deep plumes in a non-Newtonian Mantle. Phys. Earth Planet. Int. 34, 56–57.
Machetel, P., Weber, P., 1991. Intermittent layered convection in a model mantle with an endothermic phase change at 670 km. Nature 350, 55–57.
Mitchell, J.F.B., 1989. The 'greenhouse' effect and climate change. Rev. Geophys. 27, 115–139.
Mitrovica, J.X., Forte, A.M., 1997. Radial profile of mantle viscosity: results from the joint inversion of convection and postglacial rebound observables. J. Geophys. Res. 102, 2751–2769.
Newsom, H.E., White, W.M., Jochum, K.P., Hofmann, A.W., 1986. Siderophile and chalcophile element abundances in oceanic basalts, Pb isotope evolution and growth of the Earth's core. Earth Planet. Sci. Lett. 80, 299–313.
Nyblade, A.A., Pollack, H.N., 1993. A global analysis of heat flow from the Precambrian terrains: implications for the thermal structure of Archean and Proterozoic lithosphere. J. Geophys. Res. 98, 12207–12218.
Ogawa, M., 1994. Effects of chemical fractionation of heat-producing elements on mantle evolution inferred from a numerical model of coupled magmatism–mantle convection system. Phys. Earth Planet. Int. 83, 101–127.
O'Neill, H.St.C., Palme, H., 1998. Composition of the silicate Earth: implications for accretion and core formation. In: Jackson, I. (Ed.), The Earth's Mantle—Composition, Structure, and Evolution. Cambridge Univ. Press, Cambridge, pp. 3–126.
O'Neill, H.St.C., Dingwell, D.B., Borisov, A., Spettel, B., Palme, H., 1995. Experimental petrochemistry of some highly siderophile elements at high temperatures, and some implications for core formation and the mantle's early history. Chem. Geol. 120, 255–273.
O'Nions, R.K., Evensen, N.M., Hamilton, P.J., 1979. Geochemical modeling of mantle differentiation and crustal growth. J. Geophys. Res. 84, 6091–6101.
Phipps Morgan, J., Morgan, W.J., Zhang, Y.-S., Smith, W.H.F., 1995. Observational hints for a plume-fed, suboceanic asthenosphere and its role in mantle convection. J. Geophys. Res. 100, 12753–12767.
Poirier, J.-P., 1991. Introduction to the Physics of the Earth's Interior. Cambridge Univ. Press, Cambridge, 264 pp.
Pollack, H.N., 1980. The heat flow from the Earth: a review. In: Davis, P.A., Runcorn, S.K. (Eds.), Mechanisms of Continental Drift. Academic Press, San Diego, CA, pp. 175–182.
Pollack, H.N., 1986. Cratonization and thermal evolution of the mantle. Earth Planet. Sci. Lett. 80, 175–182.
Pollack, H.N., Hurter, S.J., Johnson, J.R., 1993. Heat flow from the Earth's interior: analysis of the global data set. Rev. Geophys. 31, 267–280.
Richards, M.A., 1991. Hotspots and the case for a high viscosity lower mantle. In: Sabadini, R., Lambeck, K., Boschi, E. (Eds.), Glacial Isostasy, Sea-level and Mantle Rheology. Kluwer Acad. Publ., Dordrecht, pp. 571–587.
Richter, F.M., 1973. Finite amplitude convection through a phase boundary. Geophys. J.R. Astron. Soc. 35, 265–276.
Riedel, M.R., Karato, S.-I., 1997. Grain-size evolution in subducted oceanic lithosphere associated with the olivine–spinel transformation and its effects on rheology. Earth Planet. Sci. Lett. 148, 27–43.
Rudnick, R., 1995. Making continental crust. Nature 378, 571–577.
Schmeling, H., Bussod, G.Y., 1996. Variable viscosity convection and partial melting in the continental asthenosphere. J. Geophys. Res. 101, 5411–5423.
Schmeling, H., Marquart, G., 1993. Mantle flow and the evolution of the lithosphere. Phys. Earth Planet. Int. 79, 241–267.
Schubert, G., 1979. Subsolidus convection in the mantles of terrestrial planets. Annu. Rev. Earth Planet. Sci. 7, 289–342.
Schwinner, R., 1920. Vulkanismus und Gebirgsbildung, ein Versuch. Z. Vulkanol. (Berlin) 5, 175–229.
Sleep, N.H., 1990. Hot spots and mantle plumes: some phenomenology. J. Geophys. Res. 95, 6715–6736.
Solheim, L.P., Peltier, W.R., 1994. Avalanche effects in phase transition modulated thermal convection: a model of Earth's mantle. J. Geophys. Res. 99, 6997–7018.
Spada, G., Sabadini, R., Yuen, D.A., Ricard, Y., 1992. Effects on post-glacial rebound from the hard rheology in the transition zone. Geophys. J. Int. 109, 683–700.
Spohn, T., Breuer, D., 1993. Mantle differentiation through continental crust growth and recycling and the thermal evolution of the Earth. In: Takahashi, E., Jeanloz, R., Rubie, D. (Eds.), Evolution of the Earth and Planets. Geophysical Monograph 74, IUGG, Vol. 14, AGU, 74, pp. 55–71.
Stacey, F.D., 1992. Physics of the Earth, 3rd edn. Brookfield Press, Brisbane, 513 pp.
Steinbach, V., Yuen, D.A., 1992. The effects of multiple phase transitions on Venusian mantle convection. Geophys. Res. Lett. 19, 2243–2246.
Steinbach, V., Yuen, D.A., Zhao, W., 1993. Instabilities from phase transitions and the timescales of mantle evolution. Geophys. Res. Lett. 20, 1119–1122.
Tackley, P.J., 1993. Effects of strongly temperature-dependent viscosity on time-dependent, three-dimensional models of mantle convection. Geophys. Res. Lett. 20, 2187–2190.
Tanaka, H., Nakazawa, K., 1993. Stochastic coagulation equation and validity of the statistical coagulation equation. J. Geomagn. Geoelectr. 45, 361–381.
Tanaka, H., Nakazawa, K., 1994. Validity of the statistical coagulation equation and runaway growth of protoplanets. Icarus 107, 404–412.
Taylor, R.S., McLennan, S.M., 1995. The geochemical evolution of the continental crust. Rev. Geophys. 33, 241–265.
van den Berg, A.P., Yuen, D.A., 1997. The role of shear heating in lubricating mantle flow. Earth Planet. Sci. Lett. 151, 33–42.
Vening Meinesz, F.A., 1956. Convective instability induced by phase transitions in the mantle. Proc. Kon. Ned. Akad. B 59, 1–22.
Walzer, U., Hendel, R., 1997a. Time-dependent thermal convec-

tion, mantle differentiation and continental-crust growth. Geophys. J. Int. 130, 303–325.
Walzer, U., Hendel, R., 1997b. Tectonic episodicity and convective feedback mechanisms. Phys. Earth Planet. Int. 100, 167–188.
Wetherill, G.W., 1986. Accumulation of the terrestrial planets and implications concerning lunar origin. In: Hartmann, W.K., Phillips, R.J., Taylor, G.J. (Eds.), Origin of the Moon. Lunar and Planetary Institute, Houston, pp. 519–550.
Williams, D.R., Wetherill, G.W., 1994. Size distribution of collisionally evolved asteroidal populations: analytical solution for self-similar collision cascades. Icarus 107, 117–128.
Worsley, T.R., Nance, R.D., Moody, J.B., 1986. Tectonic cycles and the history of the Earth's biogeochemical and paleoceanographic record. Paleoceanography 1, 233–263.
Zhang, S., Christensen, U.R., 1993. Some effects of lateral viscosity variations on geoid and surface velocities induced by density anomalies in the mantle. Geophys. J. Int. 114, 531–547.
Zhang, Y.-S., Tanimoto, T., 1991. Global Love wave phase velocity variation and its significance to plate tectonics. Phys. Earth Planet. Int. 66, 160–202.
Zhou, H., 1996. A high-resolution P-wave model for the top 1200 km of the mantle. J. Geophys. Res. 101, 27791–27810.